Zoological Journal of the Linnean Society, 2026, **206**(3), zlag002
https://doi.org/10.1093/zoolinnean/zlag002

OXFORD

Original Article

Phylogenetic assessment and taxonomic description of the first scale-feeding candiru from west of the Andes (Siluriformes, Trichomycteridae)

Carlos DoNascimiento[1,*], Armando Ortega-Lara[2], Juan G. Albornoz-Garzón[3], César Román-Valencia[4], Nathan K. Lujan[5]

[1]Grupo de Ictiología (GIUA), Instituto de Biología, Universidad de Antioquia, Medellín, 050010, Colombia
[2]Grupo de Investigación en Peces Neotropicales, Fundación para la Investigación y el Desarrollo Sostenible FUNINDES, Cali, 760044, Colombia
[3]Department of Ecology and Evolutionary Biology, University of Michigan, Ann Arbor, MI, 48109-1085, United States
[4]Laboratorio de Ictiología, Universidad del Quindío, Armenia, 630001, Colombia
[5]Department of Natural History, Royal Ontario Museum, and Department of Ecology and Evolutionary Biology, University of Toronto, Toronto, M5S 2C6, Canada

*Corresponding author. Grupo de Ictiología (GIUA), Instituto de Biología, Universidad de Antioquia, Medellín, 050010, Colombia. E-mail: c.donascimiento@udea.edu.co

ABSTRACT

Among vertebrates, specialized scale-feeding occurs almost exclusively in tropical freshwater fishes, with the Amazon basin having the richest regional assemblage of such specialists. With 28 valid species and 11 valid genera, 10 of which are ectoparasitic scale and mucus-feeders, the Neotropical trichomycterid subfamily Stegophilinae is the only fish lineage to have significantly diversified within this niche. Stegophilines are widespread and ubiquitous throughout the lowland freshwaters of South America, east of the Andes. We describe ***Arhinoglanis* gen. nov.** and ***Arhinoglanis relictus* sp. nov.**, the first Stegophilinae from west of the Andes, from the upper Cauca River drainage, Colombia. At 26.4 mm maximum standard length, the new genus and species is also the first miniature Stegophilinae. Using diaphanization, light microscopy, and micro-computed tomography imagery, we coded 534 morphological characters for 50 terminal taxa to recover the new taxon as sister to the exclusively cis-Andean clade of *Homodiaetus* + *Schultzichthys*. A single unique synapomorphy unites these genera: proximal tip of ceratobranchial 5 wider than proximal tip of ceratobranchial 4. Five autapomorphies diagnose the new genus, the most notable of which is a paedomorphically unossified dorsal lamina of the mesethmoid. The scarcity and highly restricted distribution of the new species within the Magdalena basin has led to its evaluation as Critically Endangered.

Keywords: catfish; Cauca River; morphology; Neotropics; Stegophilinae; systematics

INTRODUCTION

Candirus are a notorious, polyphyletic assemblage of South American catfishes defined by specializations for feeding on the dead flesh (carrion) or living blood, scales, or skin of other vertebrates. They include members of two distantly related clades: the subfamily Cetopsinae in the family Cetopsidae and the sister subfamilies Stegophilinae and Vandelliinae in the family Trichomycteridae. Candiru notoriety is generally rooted in their alleged invasion of the urethra of unaware bathers in waters of the Amazon basin (Bauer 2013). However, many of these reports are dubious. To the extent that there is any truth in these reports, the purported behaviour is exclusively associated with species of the vandelliine genus *Vandellia* Valenciennes, 1846, which, like other Vandelliinae, are obligate blood-feeders as adults (de Pinna 1998, Spotte *et al.* 2001, DoNascimiento and de Pinna 2025). In contrast, most members of Stegophilinae feed on the skin, scales, or mucus of other fishes. One species with exceptionally specialized dentition and skull morphology (*Pareiodon microps* Kner, 1855) feeds on carrion (de Pinna 1998, de Pinna and Wosiacki 2003), as do the Cetopsinae candirus [*Cetopsis candiru* Spix & Agassiz, 1829 and *Cetopsis coecutiens* (Lichtenstein, 1819)], perhaps contributing to the conflation of these fishes under a shared common moniker of candirus, despite their polyphyly.

Received 12 April 2025; revised 3 September 2025; accepted 5 January 2026
[Version of Record, first published online 10 March 2026, with fixed content and layout in compliance with Art. 8.1.3.2 ICZN. https://zoobank.org/urn:lsid:zoobank.org:pub:407334BD-B82D-4245-A936-71D5C0A4B4F0].

Monophyly of Stegophilinae is well supported based on both morphological (Datovo and Bockmann 2010, DoNascimiento 2015) and molecular evidence (Fernández and Schaefer 2009, Ochoa *et al.* 2020), and the subfamily is defined by osteological synapomorphies of the mandibular and suspensorial arches, but more conspicuously by having a mouth that forms a wide, non-occluding, crescent-shaped orifice (secondarily reversed in *Pareiodon*) (DoNascimiento 2015). Stegophilinae encompasses a broad morphological diversity that is partially reflected by it having the most genera of any Trichomycteridae subfamily, five of which are monotypic: *Acanthopoma* Lütken, 1892, *Apomatoceros* Eigenmann, 1922, *Haemomaster* Myers, 1927, *Megalocentor* de Pinna & Britski, 1991, and *Pareiodon* Kner, 1855. Stegophilines typically inhabit lowland rivers of the main cis-Andean basins of tropical South America: Amazon, Essequibo, Orinoco, Paraná-Paraguay, and São Francisco, with a few known species of *Homodiaetus* Eigenmann & Ward, 1907 restricted to coastal rivers of southeastern Brazil (Koch 2002, DoNascimiento 2015). Despite the distinctive and intriguing ecologies of these fishes, research on stegophiline diversity has progressed slowly, with extended publication intervals between major taxonomic analyses (de Miranda Ribeiro 1946, de Pinna and Britski 1991, Koch 2002, DoNascimiento and Provenzano 2006). Interestingly, several putative new species have been reported from various regions with otherwise relatively well-known ichthyofaunas (Brazil: Wosiacki and de Pinna 2007; Madeira drainage: de Pinna 2013; Guyana: Taphorn *et al.* 2022), but many of these remain undescribed.

In an unpublished dissertation, DoNascimiento (2013) briefly discussed the possible phylogenetic affinities and biogeographical implications of an undescribed stegophiline coming from the upper Cauca River in Colombia. At that time, only one specimen was available for study, precluding a comprehensive morphology-based assessment of its phylogenetic relationships. DoNascimiento (2013) tentatively placed the species as *incertae sedis* within the Stegophilinae clade containing *Homodiaetus* + *Schultzichthys* + members of the *Pareiodon* group. However, within this clade, the undescribed species was also recognized as possibly more closely related to *Homodiaetus*, based on its anteriorly placed pelvic fins, and overlapping numbers of oral teeth and odontodes, along with general phenetic resemblance. Later, additional specimens of this undescribed species were reported from the La Vieja and Risaralda rivers in the Cauca River drainage, Colombia, as an undescribed species of *Homodiaetus* (Román-Valencia *et al.* 2018), or as an undescribed species of uncertain genus in Stegophilinae (Ortega-Lara *et al.* 2022a, b). In this study, we describe this new genus and species, illustrate its internal skeletal anatomy using micro-computed tomography, infer its phylogenetic placement using a cladistic analysis of morphological characters, and discuss both the species' apomorphies and its isolated biogeographical distribution based on that phylogenetic analysis.

MATERIALS AND METHODS

All specimens examined as comparative material were already available and catalogued in ichthyological collections, while specimens of the new taxon were collected in compliance with national animal welfare laws, guidelines, and/or policies effective on the collection date of specimens under Convenio de Asociación No. 0022 of 2021, between Corporación Autónoma Regional del Valle del Cauca (CVC) and Fundación FUNINDES. Comparative examined material is listed in DoNascimiento (2015) and DoNascimiento *et al.* (2014a,b). Institutional acronyms follow Sabaj (2022).

Anatomical terminology follows references listed by anatomical complex or region in DoNascimiento (2015), except for the supracleithrum and posttemporal, which follow Kubicek (2022). We follow de Pinna *et al.* (2020) in use of the term barbular for the neomorphic sesamoid bone anterodorsal to the orbit in many trichomycterids, previously described as the tendon-bone supraorbital (Baskin 1973) or sesamoid supraorbital (Adriaens *et al.* 2010). Following de Pinna and Dagosta (2022), we use the term odontodophore for each opercular and interopercular plate supporting odontodes, labial bursa for the soft tissue pocket enclosing the claw-shaped premaxillary teeth of vandelliines, and scalpelloid for these claw-shaped premaxillary teeth, with the slight expansion of this term to apply equally to the similarly shaped oral teeth found in *Pareiodon*. Specimens were cleared and double-stained for cartilage and bone (cs) following Datovo and Bockmann (2010). Micro-computed tomographs (CT) were obtained at varying resolutions (6.05–34.88 μm) using either a GE vjtomejx s240 dual tube 240/180 kV system (General Electric, Fairfield, CT, USA) or a SkyScan 1172 (Bruker, Kontich, Belgium) and were segmented and rendered using VGStudio MAX software (Volume Graphics, Heidelberg, Germany).

Definitions of measurements follow de Pinna and Britski (1991), except for head length (HL), which follows DoNascimiento and Provenzano (2006). Measurements were obtained from digital photographs taken with a Leica MC 190 HD camera attached to a Leica S8APO stereomicroscope, using the Leica Application Suite v.3.3.0. Standard lengths (SL) are given in mm, whilst subunits of the body and head are expressed as percentages of SL and HL, respectively. Counts follow de Pinna and Dagosta (2022), except for fin ray counts, which follow Datovo *et al.* (2016). Number of procurrent dorsal- and anal-fin rays were determined using cs and CT specimens, while procurrent caudal-fin rays were counted only in the single cs paratype, since the weakly ossified or entirely cartilaginous anterior procurrent rays were poorly resolved or invisible in the CT imagery. Odontodes could be counted in all available specimens (even ethanol preserved), since they are few in number, and easy to see under a stereomicroscope. Holotype meristics are indicated by an asterisk. Counts of branchiostegal rays, vertebrae, ribs, pterygiophores, relative position of dorsal, anal, and pelvic fins, and observations of caudal skeleton elements were obtained from both cs and CT specimens. Vertebral counts include only post-Weberian vertebrae, with the compound caudal centrum (PU_1 + U_1) being counted as a single element (Lundberg and Baskin 1969). Pharyngeal teeth were counted only in the cs paratype.

The data matrix, consisting of 534 morphological characters coded for 50 terminal taxa (Supporting Information, Material S1), was assembled in Mesquite v.4.02 (Maddison and Maddison 2025) and analysed with equal weights, using a heuristic search strategy in TNT v.1.6 (Goloboff and Morales 2023). Node support values were also calculated in TNT. The 50 terminal taxa were the same used in DoNascimiento (2015). The analysis was rooted in *Nematogenys inermis* (Guichenot, 1848), based on its

sister-group relationship to Trichomycteridae (de Pinna 1992, Arcila *et al.* 2017, Betancur-R *et al.* 2017). Multistate characters and particularly those related to meristic variables, were treated as non-additive and unordered (i.e. equal probability of change among all states), taking into consideration the arguments presented by Sidlauskas and Vari (2008). Ranges of variation in meristic and continuous characters were either discretized based on observed intraspecific variation or coded according to ranges cited in the literature (an admittedly subjective coding strategy). However, we provide recorded ranges of all meristic characters for each terminal species analysed (Supporting Information, Material S1), allowing readers to implement their own coding strategies. Detailed descriptions of characters and methods for phylogenetic analysis will be provided in a forthcoming contribution by the first author; however, the complete list of characters including their corresponding number of steps, and consistency and retention indices obtained in the most parsimonious hypothesis is provided in Supporting Information, Material S2. Characters relevant to the phylogenetic relationships and monophyly of the new taxon proposed here are fully described and discussed in detail, following the same enumeration assigned by TNT (i.e. starting from character 0). Characters previously proposed by other authors are followed by their corresponding first citation in the literature enclosed in parenthesis, even in those cases where character and state definitions are not exactly the same as implemented here.

Red list assessment of the new species was carried out in accordance with the guidelines of the IUCN [International Union for Conservation of Nature (IUCN) 2024], ensuring compliance with the fundamental requirements: definition of the taxonomic level (criterion 2.1.1, taxonomic scale of categorization), precision in the geographical distribution (criterion 2.1.2, geographical scale of categorization), and verifiable data quality. Estimated extent of occurrence (EOO) and area of occupancy (AOO), based on the georeferenced records were calculated using GeoCat (https://geocat.iucnredlist.org/), defining grids of 1 km^2 (Bachman *et al.* 2011, Bachman and Moat 2012).

RESULTS

Phylogenetic analysis

Strict parsimony analysis of the data matrix of 534 characters for 50 terminal taxa yielded a single most parsimonious tree of 1412 steps with Consistency Index (CI) = 0.445 and Retention Index (RI) = 0.771 (Fig. 1). This tree showed a similar arrangement to the topology obtained by DoNascimiento (2015), recovering a monophyletic Stegophilinae, but differing by having all internal relationships completely resolved. The new genus was placed as the sister group of a clade consisting of *Homodiaetus* + *Schultzichthys*, and this whole clade was sister to the *Pareiodon* group (DoNascimiento 2015). However, node support for the clade containing

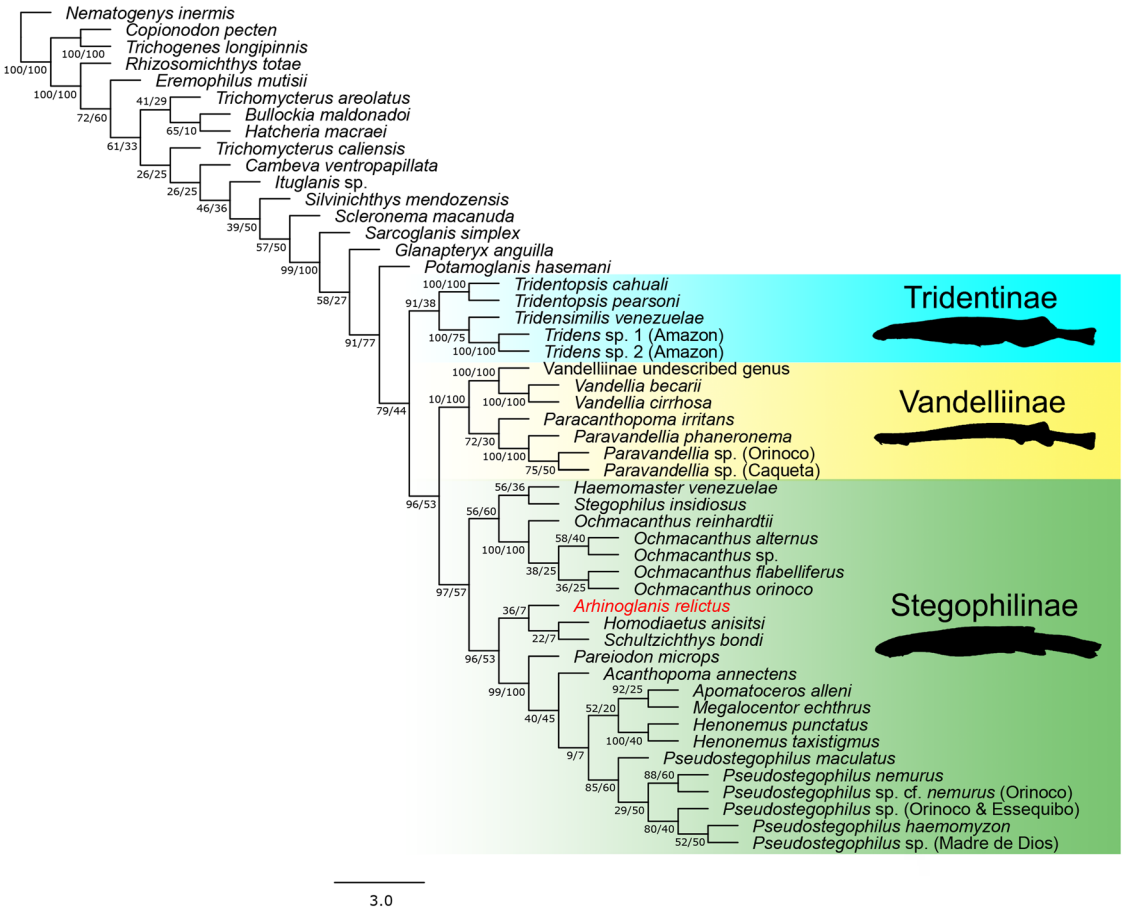

Figure 1. Single most parsimonious tree of length 1412 steps, consistency index 0.445, and retention index 0.771, depicting relationships among Stegophilinae and outgroups, generated in TNT. Numbers at nodes represent values of symmetric resampling group frequency/relative Bremer.

the new genus, *Homodiaetus*, and *Schultzichthys* was rather weak (relative Bremer support = 7; symmetric resampling group frequency = 36), as were support values for the sister pair of *Homodiaetus* and *Schultzichthys* (relative Bremer support = 7; symmetric resampling group frequency = 22). The Stegophilinae clade that included the new genus, *Homodiaetus*, *Schultzichthys*, and the *Pareiodon* group obtained stronger support (relative Bremer support = 53; symmetric resampling group frequency = 96). In contrast, the *Pareiodon* group was the best supported suprageneric clade within Stegophilinae (relative Bremer support = 100; symmetric resampling group frequency = 99). This phylogenetic analysis optimized 20 character-state changes as diagnostic for the new species (Supporting Information, Material S3), five of which corresponded to autapomorphies, justifying the erection of a new genus as detailed in the following diagnosis.

SYSTEMATICS

Trichomycteridae
Stegophilinae

Arhinoglanis gen. nov.

(Figs. 2–10)

ZooBank registration: urn:lsid:zoobank.org:act:379F5D16-4B4E-4AEF-A716-2C4DE68F4E4A.

Type species: Arhinoglanis relictus.

Diagnosis: A stegophiline trichomycterid apomorphically defined by: (i) lack of an ossified dorsal lamina of the mesethmoid, articulating with the frontal bones posteriorly (Fig. 2); (ii) anterior process of the supracleithrum forming a flat laminar expansion, roughly rectangular in shape (Fig. 3); (iii) teeth of the median premaxilla arranged in three transverse rows, occupying the entire ventral surface of the bone; (iv) unique shape (paired butterfly wings) of basibranchial 4 (Fig. 4); and (v) posterior nostril lacking surrounding flap of integument (Fig. 5). *Arhinoglanis* is further distinguished from remaining stegophilines by the following characters optimized as informative within the subfamily: (i) cranial orifice receiving the dorsal process of cleithrum absent (Figs. 3, 6); (ii) medial process of supracleithrum absent (Figs. 3, 6); (iii) lateral region of epioccipital expanded ventrally and exposed in the ventral surface of neurocranium (Fig. 6); and (iv) posterolateral process of pterotic absent (Fig. 3).

Arhinoglanis can be further distinguished by the following unique combination of characters among stegophilines: mouth ventral (Fig. 5) (vs. subterminal in *Pareiodon*); rows of small labial teeth medially continuous (Fig. 6) (vs. medially interrupted by patch of larger teeth in *Haemomaster*, *Henonemus*, and *Stegophilus*); 4–6 rows of labial teeth (vs. 2 in *Stegophilus*; 2–3 in *Pseudostegophilus maculatus* and *Pseudostegophilus haemomyzon*; 3 in *Henonemus*; 7–10 in *Haemomaster*); 4 rows of premaxillary teeth (vs. 2 in *Pareiodon*; 5 in *Haemomaster* and *Megalocentor*; 5–6 in *Apomatoceros*); 5 rows of dentary teeth (vs. 2 in *Pareiodon*; 4 in *Apomatoceros*; 6 in *Megalocentor*; 6–7 in *Henonemus punctatus*; 6–8 in *Acanthopoma*; 7–11 in *Haemomaster*; 8–9 in *Haemomaster taxistigmus*); eye dorsolateral (Fig. 5) (vs. lateral in *Apomatoceros* and *Haemomaster*); 5–8 opercular odontodes (vs. absent in *Apomatoceros* and *Megalocentor*; 2–3 in *Henonemus*); 5–7 interopercular odontodes (vs. 1–2 in *Megalocentor*; 9 in *Pseudostegophilus maculatus*; 11 in *Acanthopoma*); branchiostegal membrane medially adnate to isthmus (vs. with a free posterior margin across isthmus in *Acanthopoma* and *Schultzichthys*); occipital region of neurocranium visible through thin translucent skin (Fig. 5) (vs. covered by thick opaque skin in all stegophilines, except *Homodiaetus* and *Schultzichthys*); caudal fin bilobed (Fig. 5) (vs. rounded in *Ochmacanthus* and *Stegophilus insidiosus*; emarginate in *Haemomaster*, *Homodiaetus*, *Schultzichthys*, *Stegophilus panzeri*, and *Stegophilus septentrionalis*), and maxilla straight along its entire length (Fig. 7) (vs. curved, broadly convex along anterior margin in remaining stegophilines).

Etymology: From the Greek *rhinos* (snout) and *glanis* (catfish), in allusion to the missing bony dorsal lamina of the mesethmoid, distinguishing this genus from all other Trichomycteridae. Gender masculine.

Arhinoglanis relictus sp. nov.

(Figs 2–12; Table 1)

ZooBank registration: urn:lsid:zoobank.org:act:101FBB49-BDDF-49C8-A0A9-78B58D8C744D.

Holotype: CZUT-IC 24378 (17.2 mm SL); Colombia, Risaralda Department, río Risaralda, La Virginia Municipality, 1.3 km downstream of confluence with quebrada Totui and 7.6 km from mouth of río Cauca, 04°53′38″N 75°53′12″W, *c.* 1253 m a.s.l.; Coll. A. Ortega-Lara, D. Fernández & J. C. Salgado, 3 Sep 2021.

Paratypes: Eight specimens, all from Colombia, Risaralda Department, upper Cauca River drainage: CIUA 8011, 1 (25.5 mm SL), preserved in absolute ethanol and stored in ultracold freezer (-80°C) for DNA extraction; collected with holotype. CZUT-IC 24382, 2 (15.0, 15.8 mm SL), 1 cs (21 mm SL); collected with holotype. ROM 112325, 1 (20.9 mm SL), CT scanned; collected with holotype. Quindío Department: IUQ 414, 1 (25.1 mm SL); La Tebaida Municipality, río La Vieja, 100 m below old Pacific railway bridge, Alambrado, 04°24′10.47″N 75°48′37.64″W, 1240 m a.s.l.; Coll. C. Román-Valencia, 12 Dec 1996. MCP 26507, 2 (20.3, 26.4 mm SL); Montenegro Municipality, río La Vieja, 100 m below pedestrian bridge in San Pablo-Puerto Alejandría, 04°34′08″N 75°51′04.99″W, 1025 m a.s.l.; Coll. C. Román-Valencia & P. Ramírez, 26 Mar 1996.

Diagnosis: As for the genus.

Description: Body relatively short (HL approximately one-fifth of SL), depressed from snout tip to pectoral-fin insertion, then markedly compressed along trunk region to caudal-fin base (Fig. 5). Cross-section of body vertically oval at midlength of pectoral fin. Dorsal profile of head convex from snout tip to end of occipital region (with gentle concave depression at interorbital level), then continuous and straight, ascending to dorsal-fin origin, straight and abruptly descending along dorsal-fin base, straight and slightly descending along anterior portion of caudal peduncle to origin of dorsal fleshy fin-fold supported by procurrent caudal-fin rays. Posterior portion of caudal peduncle spatulate, with fleshy fin-folds straight and diverging posteriorly to connection with unbranched principal rays of caudal fin. Ventral profile of body almost straight from mandible to pectoral-fin base, broadly convex to anal-fin origin, then almost straight and descending along anal-fin base and

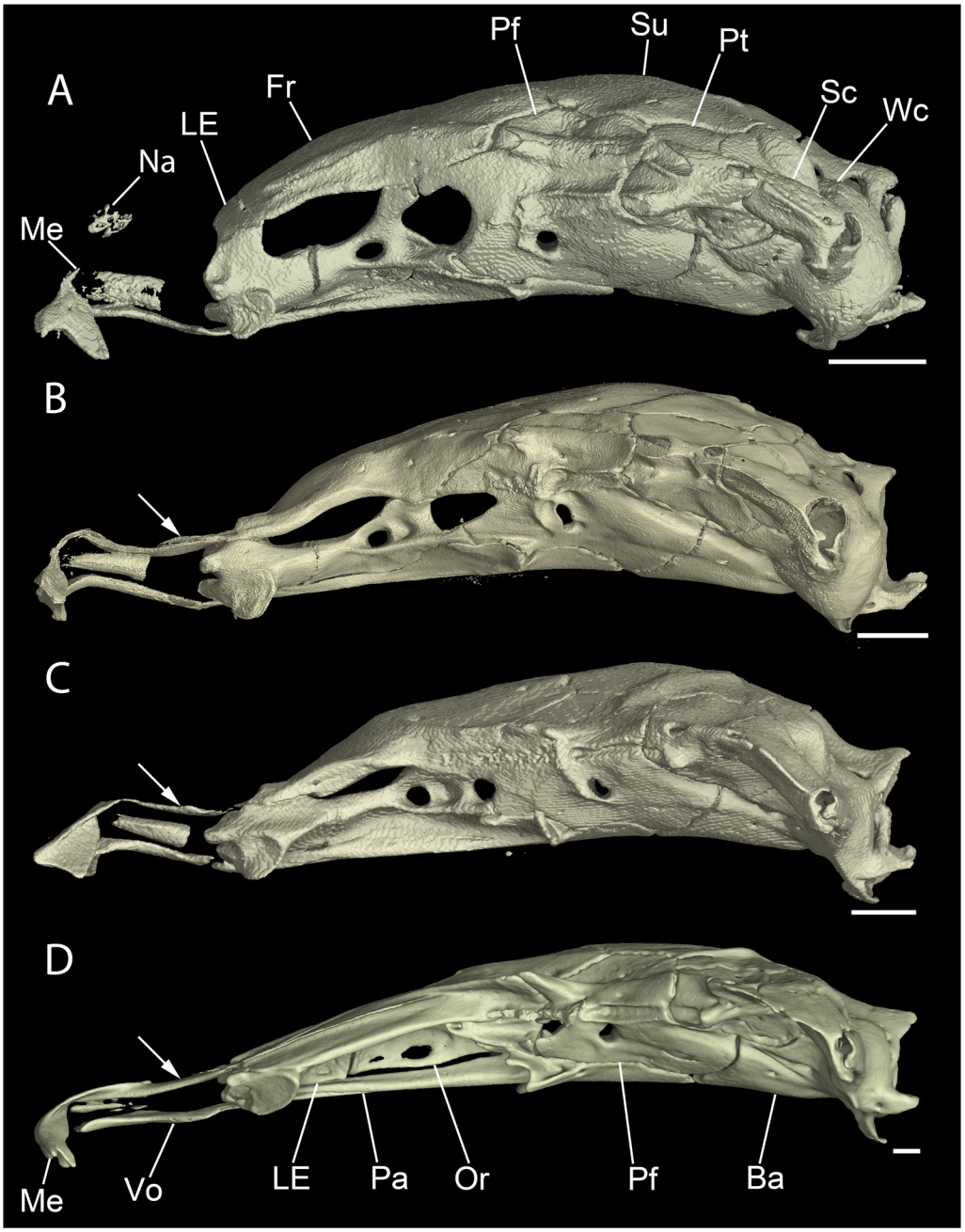

Figure 2. Lateral view of the neurocrania of (A) *Arhinoglanis relictus*, ROM 112325, paratype, 20.9 mm SL; (B) *Homodiaetus anisitsi*, CAS 37276, holotype, 34.9 mm SL; (C) *Schultzichthys bondi*, ANSP 180488, 40 mm SL; (D) *Acanthopoma annectens*, ANSP 181146, 104 mm SL. Arrows point to the dorsal lamina of the mesethmoid. Abbreviations: Ba, basioccipital+exoccipitals; Fr, frontal; LE, lateral ethmoid; Me, mesethmoid; Na, nasal; Or, orbitosphenoid; Pa, parasphenoid; Pf, pterosphenoid+sphenotic+prootic; Pt, pterotic; Sc, supracleithrum; Su, supraoccipital; Vo, vomer; Wc, Weberian capsule. Scale bars = 0.5 mm.

anterior portion of caudal peduncle to ventral fleshy fin-fold supported by procurrent caudal-fin rays. Greatest body depth at vertical through pelvic-fin origin. Myotomes evident along trunk, becoming narrower and more horizontally sloped caudally. Horizontal skeletal septum evident in preserved specimens as a conspicuous sulcus in anterior portion of body, and posteriorly traced by chromatophores along midlateral line. Axillary gland conspicuous, bulging laterally from lateral profile as large elongate and ovoid-shaped sac located immediately dorsal to pectoral fin. Axillary gland pore evident as a horizontal slit slightly behind centre of gland in lateral view.

Head depressed, as long as wide, its profile in dorsal view semicircular (Fig. 5). Snout short and broadly rounded. Mouth ventral, non-occlusive and wide, its maximum width slightly less than head width at same level. Mouth corners directed slightly posterolaterally. Mouth opening crescent shaped. Lower lip wide and thick, with pair of conspicuous triangular labial folds at corners. Upper lip with up to six rows of teeth medially, only two complete rows reaching lateral corners, supported exclusively by soft tissue of lip; three posteriormost rows continuous medially with slightly larger teeth directly inserted on median premaxilla. Median premaxilla

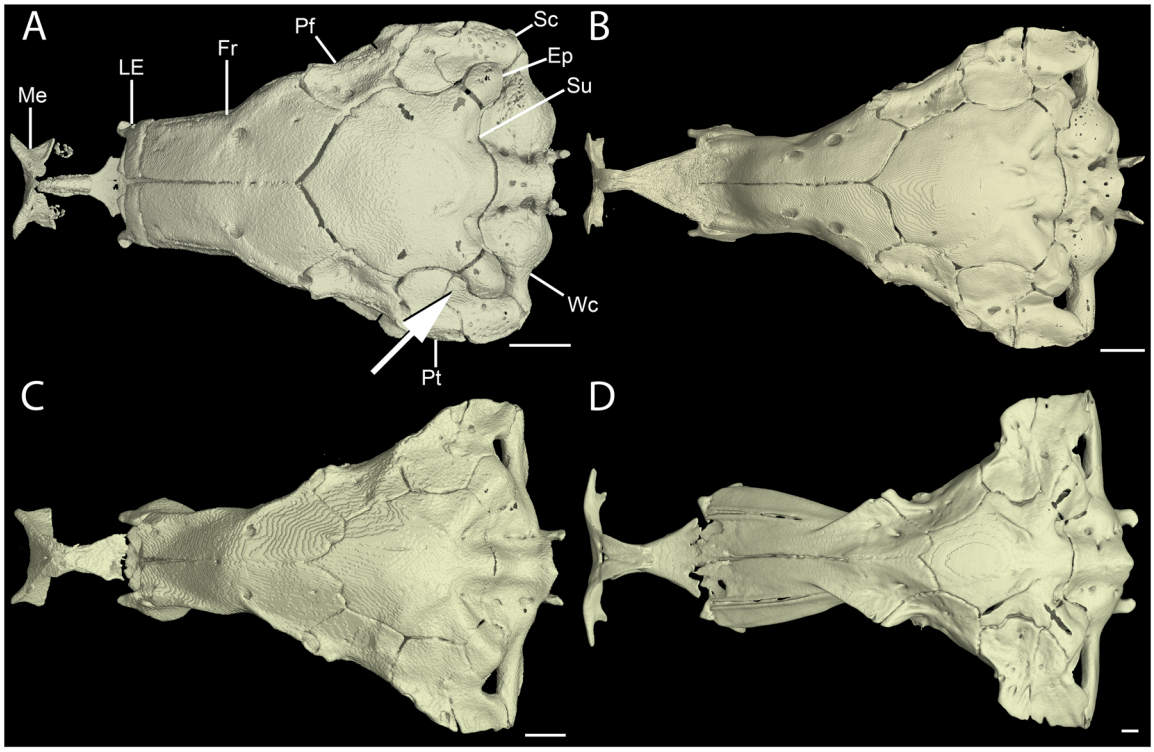

Figure 3. Dorsal view of the neurocrania of (A) *Arhinoglanis relictus*, ROM 112325, paratype, 20.9 mm SL; (B) *Homodiaetus anisitsi*, CAS 37276, holotype, 34.9 mm SL; (C) *Schultzichthys bondi*, ANSP 180488, 40 mm SL; (D) *Acanthopoma annectens*, ANSP 181146, 104 mm SL. Arrow points to the anterior process of the supracleithrum. Abbreviations: Ep, epioccipital; Fr, frontal; LE, lateral ethmoid; Me, mesethmoid; Pf, pterosphenoid+sphenotic+prootic; Pt, pterotic; Sc, supracleithrum; Su, supraoccipital; Wc, Weberian capsule. Scale bars = 1 mm.

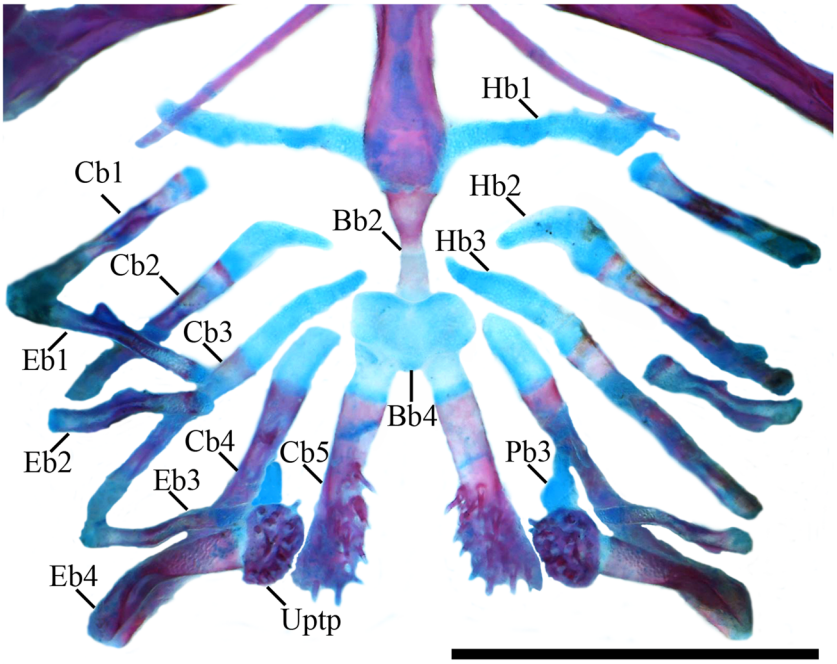

Figure 4. Dorsal view of the branchial arches of *Arhinoglanis relictus*, CZUT-IC 24382, paratype, 21 mm SL. Abbreviations: Bb2, 4, basibranchials 2, 4; Cb1–5, ceratobranchials 1–5; Eb1–4, epibranchials 1–4; Pb3, pharyngobranchial 3; Hb1–3, hypobranchials 1–3; Uptp, upper dentigerous tooth plate. Scale bar = 1 mm.

supporting three complete rows of teeth occupying entire ventral surface of bone. Premaxilla with four rows of teeth; teeth of anterior rows almost straight, bent only slightly at tip, those of posteriormost row slightly larger and more strongly S shaped. Dentary with five rows of teeth; dentary tooth rows progressively longer posteriorly, most anterior row with only 6–7 teeth, extending

Figure 5. Left lateral, dorsal, and ventral views of *Arhinoglanis relictus*, holotype, CZUT-IC 24378, 17.2 mm SL. Scale bar = 1 cm. Photographs by J.L. Londoño-López, used with permission.

from mental symphysis to half-length of second row, second row reaching laterally half-length of mandible, only two posteriormost rows complete, spanning entire mandibular length. Dentary teeth similar in shape and size to premaxillary teeth. Branchial opening small, lateral, extending from upper third of interopercular odontodophore to mid-distance between interopercular and opercular odontodophores. Branchiostegal membrane medially united to isthmus, forming short laterally-free fold. Branchiostegal rays four (Fig. 8). Upper pharyngeal tooth plate with 12 or 13 short conical teeth, arranged in two irregular rows. Ceratobranchial 5 with 11–13 teeth, similar to those of upper pharyngeal tooth plate, arranged in three irregular rows. Eye large (*c.* one-third of HL) and circular, without free orbital rim, located dorsolaterally and slightly anterior to middle of head length. Interorbital distance slightly wider than horizontal eye diameter. Interopercle with 6* or 7 posteriorly oriented and mostly straight odontodes of similar size, barely bent medially at tip, inserted at same plane in radial arrangement. Periodontodal folds of interopercular and opercular odontodophores connected through broad posteriorly concave ridge; each fold extending posteriorly scarcely beyond tip of posteriormost odontodes. Opercle with 6*–8 posteriorly oriented odontodes, arranged in three antero-posterior irregular series, largest odontodes in posteriormost row; odontodes mostly straight, except odontodes of posteriormost row with slightly bent tip. Maxillary barbel broad at base, tapering to tip, reaching posterior margin of interopercular periodontodal fold. Rictal barbel extending two-thirds of length of maxillary barbel. Anterior nostril small, encircled by low tubular fleshy membrane, posteriorly folded. Posterior nostril approximately twice as large as anterior nostril and transversely oriented as oval opening, located medially to anterior region of eye, its anterior margin behind anterior margin of eye, separated from anterior nostril by about same distance as separates posterior nostrils. Borders of posterior nostril continuous with skin of head, lacking fleshy membrane.

Supraorbital sensory pore (s1) located medial to posterior margin of anterior nostril, joined through short membranous tubule (partially ossified, open dorsally) to second supraorbital sensory pore (s2), opening medial to anteromedial corner of posterior nostril. Epiphysial sensory pore (s6) paired, slightly closer to dorsal midline than eye, at level with posterior margin of eye. Posteriormost sensory pore of infraorbital canal (i11) located behind eye. Terminal pore of short preopercular branch (preop) opens anteroventral to opercular odontodophore. Sensory pore at end of short pterotic branch of postotic canal (pt.br) located dorsally to opercular odontodophore. First lateral-line pore (ll1) emerges immediately dorsal to approximately middle region of axillary gland. Lateral-line canal conspicuous as translucent layer above axillary gland, extending to middle length of adpressed pectoral fin (not reaching posterior margin of axillary gland). Ossified tubule of lateral-line canal short but completely closed, located just posterior to ventral branch of ll1 pore.

Pectoral fin i, 5, first ray slightly thicker than remaining rays, tips of branched rays projected slightly beyond fin membrane. Distal margin of pectoral fin almost straight. Pelvic fin i, 4, with short pelvic splint lateral to first ray; medial bases of fins well separated, inserted anterior to dorsal-fin origin, slightly closer to snout tip than to base of caudal fin, at vertical through free vertebra 13 or 14. Distal margin of pelvic fin round, reaching urogenital opening. Dorsal fin triangular in lateral aspect, with ii–iii^{P}, ii, 7; first branched ray longest. Dorsal-fin pterygiophores eight, inserted between neural spines of free vertebrae 16–21 or 22 (Fig. 9). Anal fin roughly rectangular in lateral aspect, with iii–iv^{P},

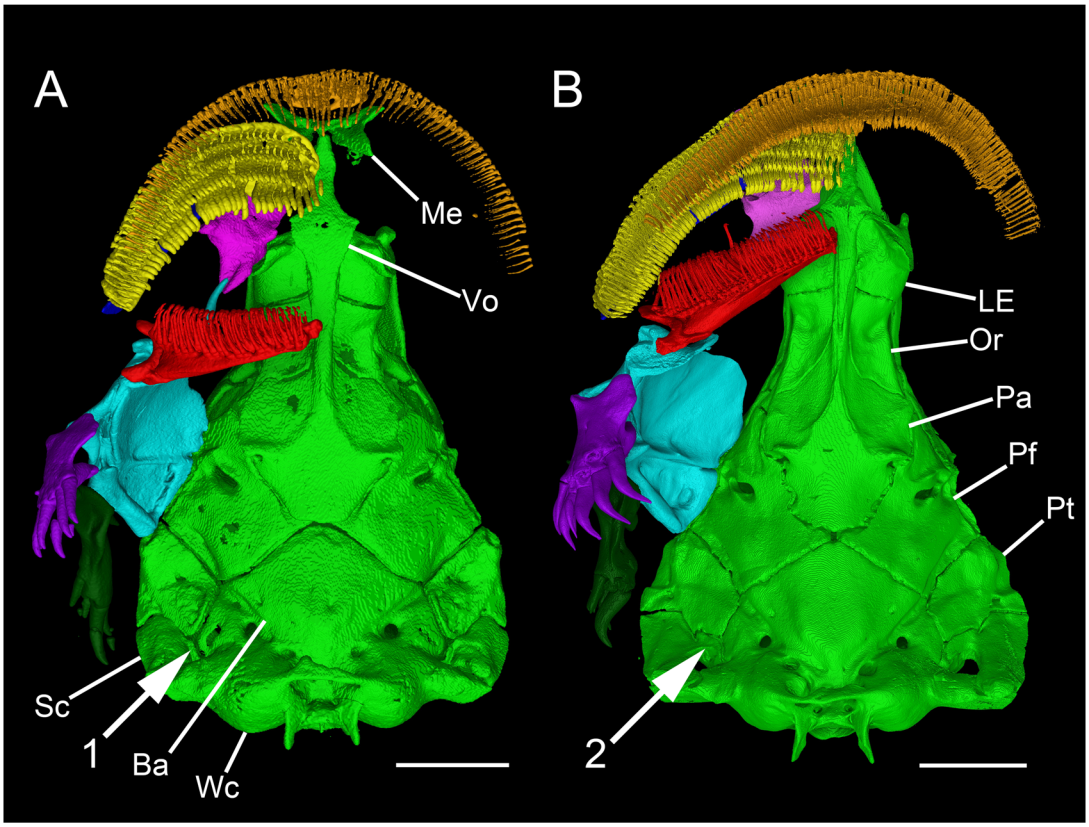

Figure 6. Ventral view of cranium of (A) *Arhinoglanis relictus*, ROM 112325, paratype, 20.9 mm SL, scale bar = 0.8 mm; (B) *Homodiaetus anisitsi*, CAS 37276, 34.9 mm SL, holotype, scale bar = 1 mm. Labial teeth (orange), premaxillary teeth (yellow), neurocranium (light green), autopalatine (light purple), lower jaw and dentary teeth (red), hyomandibula and quadrate (blue), interopercle (dark purple), opercle (dark green). Components of upper and lower jaws, suspensorium, and opercular series of left side removed. Arrow 1 points to the ventrally exposed surface of lateral region of epioccipital and arrow 2 points to the medial process of supracleithrum. Abbreviations: Ba, basioccipital+exoccipitals; LE, lateral ethmoid; Me, mesethmoid; Or, orbitosphenoid; Pa, parasphenoid; Pf, pterosphenoid+sphenotic+prootic; Pt, pterotic; Sc, supracleithrum; Vo, vomer; Wc, Weberian capsule.

ii, 5; third ray (first branched) longest. Anal-fin origin behind dorsal-fin origin, at vertical between bases of third (first branched) and fourth dorsal-fin rays. Anal-fin pterygiophores six, inserted between hemal spines of free vertebrae 18–23 (Fig. 9). Caudal fin bilobed with i, 5 + 6, i rays, both lobes round, upper lobe slightly longer. Procurrent caudal-fin rays 21 dorsally (only posteriormost 4 rays ossified and last ray also segmented, articulating with distal tip of uroneural) and 23 ventrally (only posteriormost 3 rays ossified, last ray also segmented, articulating with ventral tip of lower hypural plate), inserted posterior to neural spine of vertebra PU_{12} and hemal spine of vertebra PU_{13}, respectively. Caudal skeleton PH + 1 + 2, 3, 4 + 5 (Fig. 9).

Free precaudal vertebrae 7 (first complete hemal spine on vertebra 8) and caudal vertebrae 33–34. CT scanned specimen (ROM 112325) with closed hemal arch on vertebra 6 and seventh vertebra having parapophyses unfused (Fig. 9). Anteriormost 5 or 6 vertebrae bearing ribs, last pair complete, rudimentary, or asymmetrical.

Colour in alcohol: Ground colour white (Fig. 5). Dorsal surface of snout with pair of anteriorly diverging chromatophore rows located between anterior nostrils. Dorsal surface of skull densely covered by inner layer of chromatophores, at interorbital and supraoccipital regions. Surface of upper lip with three irregular rows of chromatophores concentrically arranged around mouth opening. Ventral surface of lower lip with patch of chromatophores at each side of lower jaw. Dorsal and ventral surface of maxillary barbel base with chromatophores. Dark spots at interopercular and opercular odontodophores. Diffuse sparse chromatophores on predorsal region of trunk. Black chromatophores closely clustered with reddish brown chromatophores along middorsal region of body, immediately posterior to dorsal-fin base. Chromatophores forming conspicuous blotches aligned with insertion of rays of dorsal (second to eight rays) and anal (third to seventh rays) fins. Chromatophores clustered along midlateral line, forming discrete black streak from above anal-fin base to caudal-fin base. Dark midlateral streak slightly wider posteriorly, along region of caudal peduncle supporting procurrent rays of caudal fin. Posterior end of dark midlateral streak separated from irregular elongated blotch on basal third of middle caudal-fin rays by hyaline slender vertical band. Sparse stellate chromatophores along sides of dorsal limit of abdominal cavity, extending from distal margin of pectoral fin to anus. Base of first pectoral-fin ray with chromatophores along anterior edge. Interradial membrane and rays of fins hyaline, except for base of dorsal, anal, and caudal fins, with pigmentation pattern already described above.

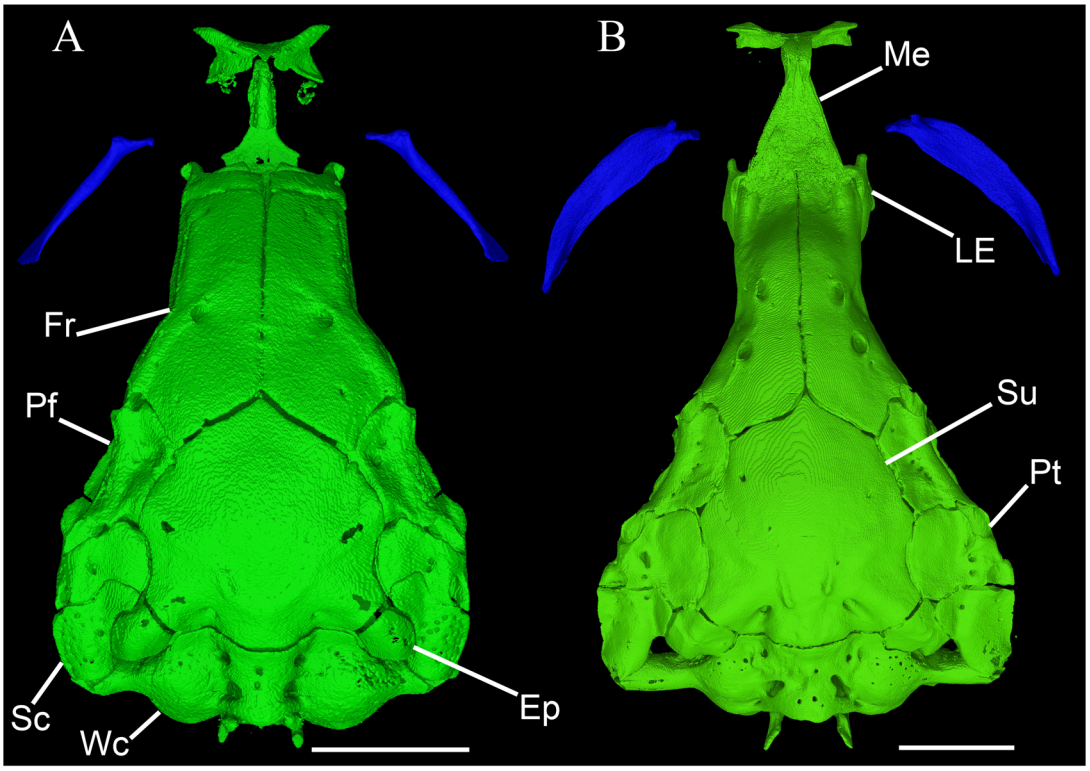

Figure 7. Dorsal view of cranium of (A) *Arhinoglanis relictus*, ROM 112325, paratype, 20.9 mm SL; (B) *Homodiaetus anisitsi*, CAS 37276, holotype, 34.9 mm SL. Maxilla showed isolated in blue. Abbreviations: Ep, epioccipital; Fr, frontal; LE, lateral ethmoid; Me, mesethmoid; Pf, pterosphenoid+sphenotic+prootic; Pt, pterotic; Sc, supracleithrum; Su, supraoccipital; Wc, Weberian capsule. Scale bars = 1 mm.

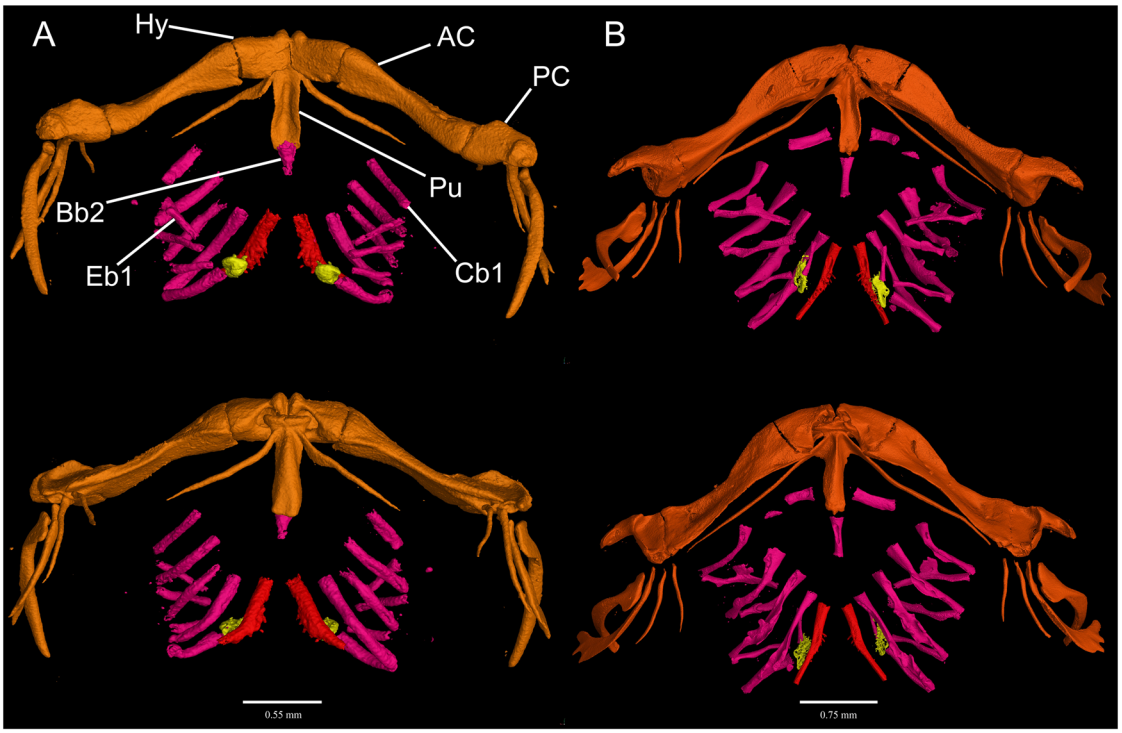

Figure 8. Dorsal (upper row) and ventral (bottom row) views of the hyoid and branchial arches of (A) *Arhinoglanis relictus*, ROM 112325, paratype, 20.9 mm SL; (B) *Homodiaetus anisitsi*, CAS 37276, holotype, 34.9 mm SL. Hyoid arch (orange), basibranchial 2, epibranchials 1–4, and ceratobranchials 1–4 (purple), ceratobranchial 5 (red), upper pharyngeal tooth plate (yellow) Abbreviations: Bb2, basibranchial 2; AC, anterior ceratohyal; Cb1, ceratobranchial 1; Eb1, epibranchial 1; Hy, hypohyal; PC, posterior ceratohyal; Pu, parurohyal. Scale bars = 1 mm.

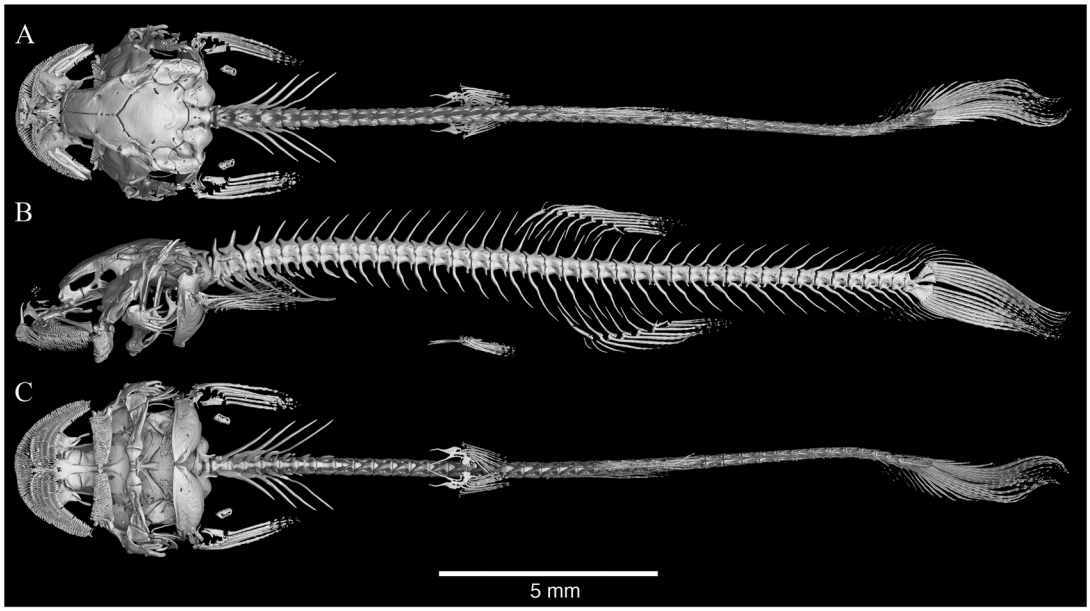

Figure 9. Skeleton of *Arhinoglanis relictus*, ROM 112325, paratype, 20.9 mm SL, in dorsal (A), lateral (B), and ventral (C) views.

Figure 10. *Arhinoglanis relictus*, live paratype, ROM 112325, 20.9 mm SL, in lateral (A) and dorsal (B) views.

Colour in life: Body white with greenish sheen (Fig. 10). Muscle layer translucent with inner longitudinal line of alternating black and golden bands running along vertebral column, black bands approximately 2–3 times longer than golden bands. A second uninterrupted longitudinal golden line almost parallel and ventral to dorsal line with conspicuous widening anteriorly, approximately above middle third of pectoral fin. Peritoneum silver with outer melanophores clustered on dorsal surface of abdominal cavity. Eye golden with black iris. Dark pigmentation as described for coloration in alcohol.

Distribution and ecological notes: Arhinoglanis relictus is only known from a relatively narrow stretch of the upper Cauca River basin, in the La Vieja and Risaralda rivers (Fig. 11). The holotype was collected in a backwater area of 1.0 m depth, sheltered from strong current, with soft sandy-muddy substrate and organic debris. Specimens from the San Pablo and Alambrado localities were found in a pool of 0.8 m width and 0.9 m depth, along the bank of the La Vieja River, with a bottom substrate of mud, stones, and organic debris, pH around 7.0, mean dissolved oxygen of 7.2 mg/1, and water temperature of 22.5° C. *Arhinoglanis relictus* was collected with *Creagrutus brevipinnis* Eigenmann, 1913, *Ichthyoelephas longirostris* (Steindachner, 1879), and *Paravandellia phaneronema* (Miles, 1943) at San Pablo, and with *Astyanax* sp., *Gephyrocharax caucanus* Eigenmann, 1912, *Saccodon dariensis* (Meek & Hildebrand, 1913), *Prochilodus magdalenae* Steindachner, 1879, and *Sturisomatichthys leightoni* (Regan, 1912) at La Virginia.

Evidence of ingested scales was found in a 20.9 mm SL paratype (ROM 112325; Fig. 12), where three white regular areas, anteroposteriorly aligned, are clearly visible through the translucent abdominal wall in the live specimen (anteriormost area lies right dorsal to a main blood vessel). CT reconstructions reveal that in each of these three areas are stacks of scales (two scales can be confidently counted in the anteriormost stack, with successive stacks having more) (Fig. 12). The longest axis of individual scales is as long as the width of the mouth in its relaxed position. Presence of scales in the alimentary canal of *Arhinoglanis relictus* is consistent with the specialized lepidophagous diet of most Stegophilinae (de Pinna 1998, Bonato *et al.* 2018, DoNascimiento and de Pinna 2025).

Conservation assessment: The estimated EOO and AOO for *Arhinoglanis relictus* are 46.03 km² (B1: less than 500 km²) and 3000 km² (B2: 5000 km²), respectively, and the number of localities where the species has been recorded are three (less than five). Subpopulations are inferred to be fragmented within their distribution area in the upper Cauca River basin, given their specialized habitat requirements and also by habitat degradation by sugarcane crops, artisanal and industrial sand extraction, as well as pollution to which these environments are subjected. Therefore, this species is categorized as Critically Endangered (CR), according to criteria B1ab (ii, iii, iv) (IUCN 2024).

Etymology: From the Latin *relictum* (relic) in reference to the isolated geographic distribution of this species as the sole member of Stegophilinae present in a trans-Andean River basin (west of the Andean Central cordillera). The specific epithet is used as an adjective.

Table 1. Morphometric data for holotype (H) and four paratypes of *Arhinoglanis relictus*. Standard length (SL) expressed in mm. Measurements expressed as % of SL or head length (HL).

	H	M[a]	R[b]	SD
Standard length	17.2	-	15.0–25.5	-
Total length (SL)	118.6	-	115.3–118.8	-
Body depth (SL)	16.6	16.0	14.8–16.7	0.8
Predorsal length (SL)	58.1	58.4	55.3–62.9	3.1
Preanal length (SL)	61.9	61.1	60.0–62.0	0.9
Prepelvic length (SL)	50.7	48.2	46.7–50.7	1.6
Caudal-peduncle length (SL)	28.8	26.9	24.0–29.7	2.3
Caudal-peduncle depth (SL)	8.9	9.0	7.4–10.7	1.2
Dorsal-fin base (SL)	10.5	11.2	10.3–12.6	0.9
Anal-fin base (SL)	10.0	9.5	7.8–10.1	1.0
Head length (SL)	19.8	20.2	19.3–21.8	1.0
Head width (HL)	90.0	89.5	85.7–92.7	2.5
Head depth (HL)	58.2	57	54.7–60.3	2.3
Snout length (HL)	36.8	35.0	32.0–37.0	2.0
Mouth width (HL)	57.1	53.3	51.5–57.1	2.2
Interorbital distance (HL)	30.0	31.1	29.8–33.7	1.6

[a]M, mean.
[b]R, range.

DISCUSSION

Phylogenetic relationships of *Arhinoglanis*

Phylogenetic relationships recovered for Stegophilinae in our analysis of morphological characters are mostly congruent with the topology obtained by the Ochoa *et al.* (2020) analysis of genome-wide ultra-conserved elements, which is the most taxonomically comprehensive molecular phylogenetic study of the subfamily to date (only *Apomatoceros* and *Schultzichthys* are missing). The single exception was the shift in the position of the clade including *Henonemus* and *Megalocentor*, which in our topology is placed as sister to *Pseudostegophilus* (albeit with negligible support values: relative Bremer = 9; symmetric resampling group frequency = 7), rather than in a sister position to the remaining genera of the *Pareiodon* group, as found congruently by DoNascimiento (2015) and Ochoa *et al.* (2020). In contrast, Fernández and Schaefer (2009) recovered, both in parsimony and maximum likelihood inferences of multilocus data, *Megalocentor* as a separate lineage,

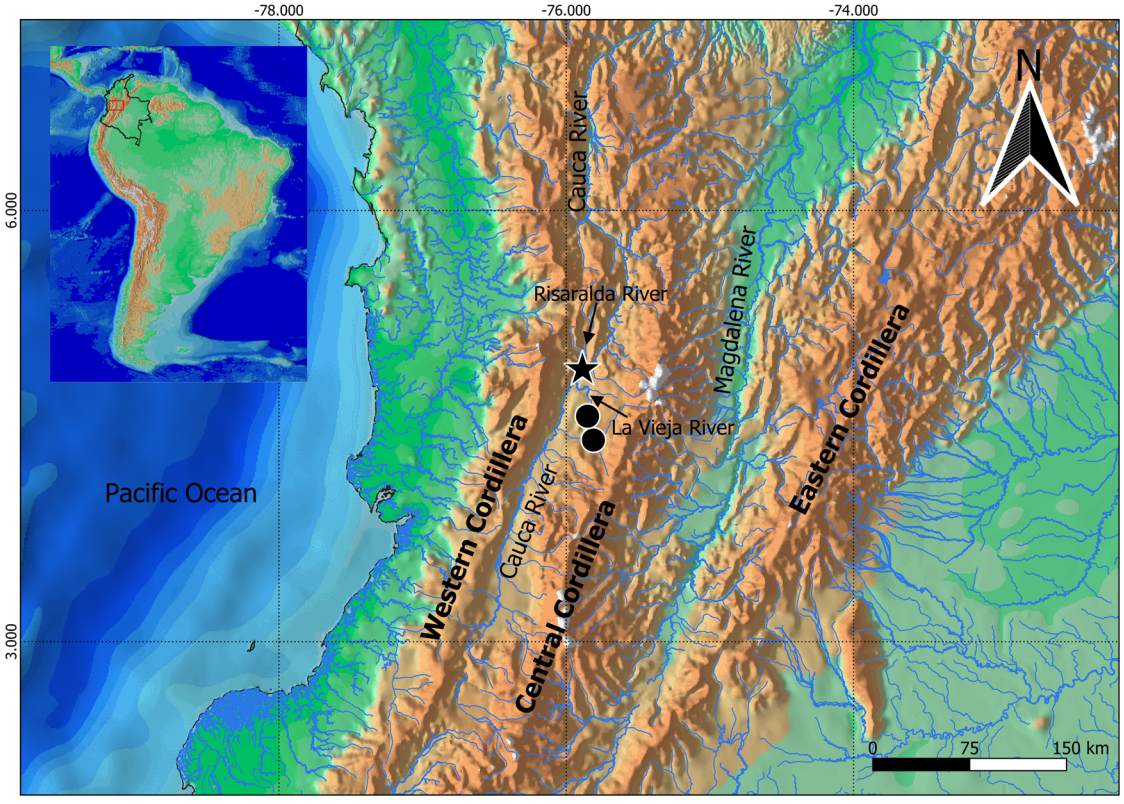

Figure 11. Map of western Colombia, showing the distribution of *Arhinoglanis relictus*. Star: type locality.

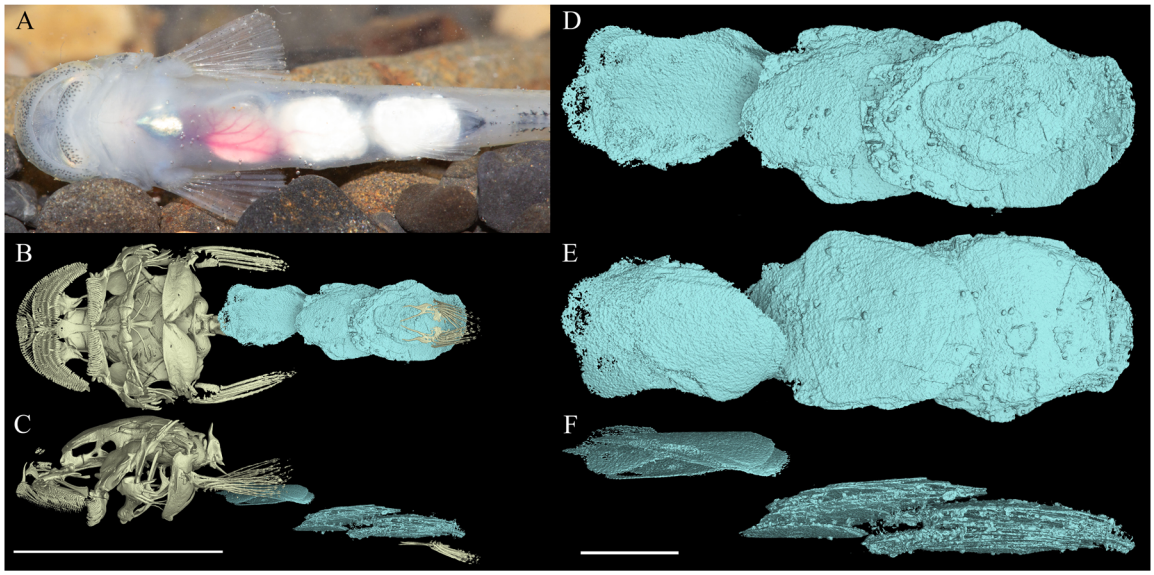

Figure 12. A, ventral photo of live paratype of *Arhinoglanis relictus*, ROM 112325, 20.9 mm SL, showing gut content, and CT reconstructions of same specimen in (B) ventral and (C) left lateral views, with magnified gut content in (D) ventral, (E) dorsal, and (F) left lateral views. Scale bars (left) = 5 mm, (right) = 1 mm.

sister to the *Pareiodon* group, and the *Apomatoceros* + *Henonemus* clade as sister to *Pseudostegophilus*, being partially congruent with our results on this last point. However, once again, the support values obtained for these arrangements are not statistically significant (bootstrap ≤ 33, jackknife ≤ 22, only provided for parsimony results), suggesting a weak phylogenetic signal associated with *Apomatoceros*, *Henonemus*, and *Megalocentor*.

Arhinoglanis is sister to the clade of *Homodiaetus* + *Schultzichthys*, with this position of the new genus being supported by a single synapomorphy exclusively shared by these three genera, character 354 (state 1): proximal tip of ceratobranchial 5 wider than proximal tip of ceratobranchial 4 (Fig. 4) (vs. the plesiomorphic state defined by tip slender or of equal width). Remaining characters recovered as informative for this node have homoplastic distributions across various taxa, accounting for the weak support obtained for this node in the parsimony analysis (Fig. 1). We will discuss each of these characters in the context of their phylogenetic information within Stegophilinae. Characters are presented by the number they are assigned in the data matrix generated by the TNT software (Supporting Information, Material S2):

Character 89 (state 1): absence of postorbital process (sphenotic spine) (Fig. 3A–C). Found also in *Apomatoceros* within Stegophilinae, *Paracanthopoma*, *Paravandellia*, and an undescribed genus in Vandelliinae, and at least *Sarcoglanis* within Sarcoglanidinae.

Character 305 (state 0): hypobranchial 2 not ossified (Figs. 2, 8). Reversed to its plesiomorphic character-state and homoplastic in *Trichogenes*, *Tridentopsis*, and at least *Glanapteryx* within Glanapteryginae. *Homodiaetus* was coded as polymorphic, given that one cs specimen (ANSP 168835: 26.3 mm SL) has a small ossification at the posterolateral corner of the left hypobranchial (this ossification pattern is unusual, since this region commonly remains cartilaginous in most species where this skeletal element is ossified), while the right hypobranchial of the same specimen is ossified at its anterolateral tip (although barely, as a minute distal bony nodule). Ossification of this element can also be asymmetrical, as in *Pseudostegophilus maculatus* (FMNH 58526) and *Pseudostegophilus haemomyzon* (MBUCV-CT-281: 53.2 mm SL, where an entirely cartilaginous left hypobranchial was observed), while in the remaining two cs specimens of *Pseudostegophilus haemomyzon* (MBUCV-CT-281: 60.3 mm SL; MBUCV-CT-778: 44.2 mm SL), both hypobranchials are similarly ossified.

Character 353 (state 0): ceratobranchial 5 similar in width to remaining ceratobranchials (Fig. 8). Reversed to its plesiomorphic character-state and broadly homoplastic in Stegophilinae (*Haemomaster*, *Henonemus*, *Megalocentor*, *Stegophilus*, and several species of *Pseudostegophilus*).

Character 380 (state 1): neural spine of compound caudal centrum present (Fig. 9). Homoplastic in *Ochmacanthus alternus* within Stegophilinae, *Scleronema* within Trichomycterinae, *Potamoglanis*, Tridentinae, *Paracanthopoma*, *Vandellia*, and an undescribed genus within Vandelliinae, and at least *Glanapteryx* within Glanapteryginae. *Schultzichthys bondi* is intraspecifically polymorphic (MBUCV-CT-916 cs specimen has a complete neural spine), as well as individually (MBUCV-CT-920 cs specimen has only left half of spine). *Ochmacanthus alternus* is also polymorphic (second-largest cs specimen of MBUCV-V-260 and MBUCV-CT-531 cs specimen both have only left half of spine).

Character 425 (state 2): medial margin of posterior region of cleithrum indented (Baskin 1973). Homoplastic in *Pseudostegophilus nemurus* and *Pseudostegophilus* sp. cf. *nemurus* (Orinoco).

Character 458 (state 3): posterior (ischiatic) process of basypterygium short and parallel to anteroposterior axis of body (Fig. 9). *Schultzichthys* is polymorphic for this character showing states 1 (short and oriented posterolaterally) and 2 (short and oriented medially).

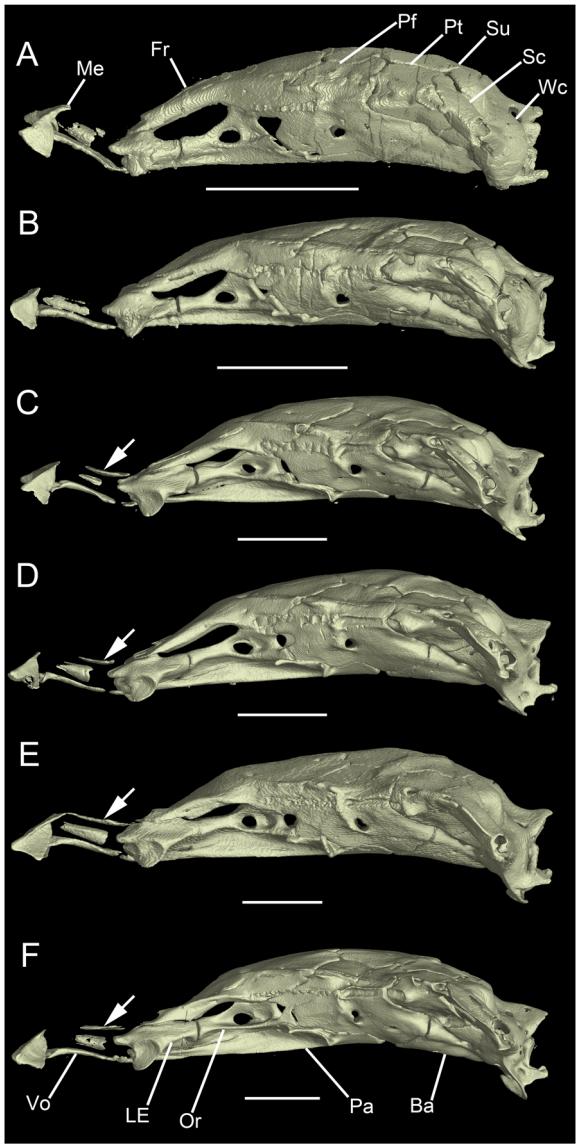

Figure 13. Lateral view of the neurocrania of *Schultzichthys bondi* showing ossification sequence of the mesethmoid: (A) AUM 41490 (Ventuari River, 18.1 mm SL); (B) AUM 53787 (Apure River, 23.3 mm SL); (C) AUM 35869 (Essequibo River, 35.8 mm SL); (D) AUM 38249 (Takutu River, 37.1 mm SL); (E) ANSP 180488 (Ireng River, 40 mm SL); (F) AUM 35430 (Meta River, 45.3 mm SL). Arrows point to the dorsal lamina of the mesethmoid. Abbreviations: Ba, basioccipital+exoccipitals; Fr, frontal; LE, lateral ethmoid; Me, mesethmoid; Or, orbitosphenoid; Pa, parasphenoid; Pf, pterosphenoid+sphenotic+prootic; Pt, pterotic; Sc, supracleithrum; Su, supraoccipital; Vo, vomer; Wc, Weberian capsule. Scale bars = 1 mm.

Autapomorphies of *Arhinoglanis*

Besides its phylogenetic position, recognition of *Arhinoglanis* is unequivocal in the form of five autapomorphies, of which the most notable is the lack of ossification of the dorsal lamina of the mesethmoid (character 5, state 1) (Fig. 2). Plesiomorphically, this bone in trichomycterids consists of a well-ossified dorsal lamina, variably wide, that expands posteriorly to articulate with the anterior end of the frontals, overlapping most of the dorsal surface of the lateral ethmoids. *Schultzichthys bondi* shows in early stages of growth a similar condition to that of *Arhinoglanis*, resulting from the late ossification of this region of the mesethmoid in the former (Fig. 13). In small specimens (18.1–23.3 mm SL), the posterior region of the mesethmoid completely lacks any sign of ossification (Fig. 13A–B). Ossification of this region initiates in the form of a thin lamina, placed immediately above the ventral endochondral ossification of the ethmoid plate as verified in specimens of 35.8–37.1 mm SL (Fig. 13C–D). This dorsal lamina is disconnected from the frontal bones and only in larger specimens (≥ 40 mm SL) is the lamina entirely ossified, meeting with the anterior region of the mesethmoid that bears the mesethmoid cornua, and fully articulated posteriorly with the frontals, showing the plesiomorphic condition of the character (Fig. 13E). However, some variation in the timing of ossification could be verified in a 45.3 mm SL specimen from the Meta River (Orinoco basin) that still shows an incomplete dorsal lamina, not connected yet with the frontals (Fig. 13F). In *Apomatoceros* and *Pareiodon*, there are two independent apomorphic conditions; a first state, where the dorsal portion of the mesethmoid is represented by a slender process as seen in *Apomatoceros*; and a second state present in *Pareiodon*, where only the posterior portion of the lamina is ossified and articulated with the frontals but remains disconnected anteriorly from the well-ossified mesethmoid cornua. Vandelliines also show a third instance of apomorphic variation of the mesethmoid that superficially resembles the condition seen in *Apomatoceros*, but differing in that the complete mesethmoid forms a slender but robust posteriorly pointed body. In any case, independently from these structural variations, this portion of the mesethmoid is always ossified in trichomycterids, its lack of ossification being exclusive to *Arhinoglanis*.

The second character-state exclusive to *Arhinoglanis* is the shape of the anterior process of the supracleithrum (rectangular) (state 3 of character 96) (Fig. 3A). When present, the anterior process of the supracleithrum is typically slender, pointed, and of variable length (depending on the taxonomic group), projects over the medial margin of the pterotic, and fits into a conspicuous notch on the dorsal surface of this latter bone. *Nematogenys* equally has an anteromedial projection of the supracleithrum over the pterotic, thus its presence is considered plesiomorphic for trichomycterids. In *Trichogenes*, *Cambeva*, and *Trichomycterus*, the process is located just medial to the base of the lateral projection of the pterotic. The orientation of the process in *Bullockia* is practically transverse to the anteroposterior axis. In *Hatcheria* and *Scleronema*, the orientation of the process is also mostly medial, and its shape is similar in both genera, being relatively wide with a truncated tip. *Ituglanis* has a comparatively shorter process; however, it is conspicuously placed over the pterotic. Most stegophilines have a wide anterior process, similar in shape to that present in *Hatcheria* and *Scleronema*, also showing the same orientation (mostly medial). In *Glanapteryx*, the process originates in a more posterior position, from the middle of the medial margin of the supracleithrum, and is transversally oriented, lying along the articulation between the pterotic and the epioccipital, with its tip reaching close to the articular cartilaginous block of the pterotic with the supraoccipital.

The arrangement of teeth of the median premaxilla is also unique for *Arhinoglanis*, consisting of three full regular transverse rows filling the entire ventral surface of the bone (character 157,

state 3). Median premaxillary teeth showing the presumed plesiomorphic character-state have an irregular distribution, clustered in a patch that occupies the entire ventral surface of the flat bone. In *Haemomaster*, *Ochmacanthus*, and *Stegophilus*, teeth of this patch are characteristically larger than labial (missing in *Ochmacanthus*) and premaxillary teeth, and interrupt medially the posteriormost row of labial teeth, while the anteriormost labial rows surround the tooth patch anteriorly in *Haemomaster* and *Stegophilus*. The derived state 1 is defined by the transverse and regular arrangement of the median premaxillary teeth, inserted along the anterior margin of the laminar bone. In *Acanthopoma*, *Apomatoceros*, *Homodiaetus*, *Megalocentor*, and *Pseudostegophilus*, median premaxillary teeth are distributed in a single regular row, continuous with the posteriormost labial row. Except for *Megalocentor*, where all median premaxillary teeth are conspicuously larger, teeth in remaining genera are similar in size to those of the posteriormost row of labial teeth. In *Schultzichthys*, the median premaxilla has two rows of teeth, with the anteriormost row being similar to that found in the other genera showing the derived state 1, i.e. aligned with the posteriormost row of labial teeth, while the second row is parallel to the anterior row and restricted to the middle portion of the bone. Finally, *Henonemus* also shows the derived state 1 and has a triangular median premaxilla, with two irregular rows restricted to the anterior margin, and teeth of the posteriormost row being larger and medially interrupting the posteriormost row of labial teeth. In the derived state 2, present in *Vandellia* and an undescribed vandelliine genus, teeth are arranged in a V formation, and are larger medially, with the central teeth thicker and longer. This single row is placed relatively posterior on the bone.

Another exclusive condition for *Arhinoglanis* is the shape of the basibranchial 4, being like that of a paired butterfly wing (state 2 of character 297) (Fig. 4). A hexagonal basibranchial 4 represents the plesiomorphic character-state for trichomycterids. Vandelliines show an alternative derived state in the form of an elongated cartilaginous rod, located between the medial tips of ceratobranchials 3 and 4, which are proximate to each other. Ceratobranchial 4 in *Vandellia* and in an undescribed vandelliine genus has an orientation similar to that commonly found in ceratobranchial 5, whose medial tips converge anteriorly, limiting posteriorly the extension of basibranchial 4.

The last autapomorphy identified for *Arhinoglanis* is the absence of a fleshy membrane encircling the posterior nostril (character 514, state 3) (Fig. 5). The plesiomophic state is defined by presence of an elevated fleshy membrane surrounding the anterior, medial, and lateral margins of the nostril, barely leaving a slender notch at its posterior margin. An uninterrupted fleshy membrane encircling the entire margin of the nostril was proposed as a synapomorphy for *Pseudostegophilus* (DoNascimiento 2015).

Next, we discuss character-state changes that are non-exclusive to *Arhinoglanis*, but are still informative for its recognition within Stegophilinae:

Character 60 (state 1): cranial orifice for insertion of dorsal process of cleithrum absent (Figs. 3A, 6A). The pectoral girdle of trichomycterids contacts the skull via insertion of a dorsal process of the cleithrum into an orifice delimited by the supracleithrum anteriorly and the Weberian capsule posteriorly. In general, the anterior margin of this orifice is exclusively defined by the supracleithrum, through the articulation of its medial process with the anterior wall of the Weberian capsule, leaving an open space between these structures. In those groups where the medial process is absent (*Tridens* and *Tridensimilis*), the orifice is delimited by the main body of the supracleithrum. Presence of this orifice represents the plesiomorphic character-state for Trichomycteridae. In the derived state, homoplastically present in the Vandelliinae clade of *Paracanthopoma*+*Paravandellia*, *Arhinoglanis*, and at least *Glanapteryx* within Glanapteryginae, the supracleithrum lacks a medial process and the bone is completely attached to the basioccipital+exoccipitals, obliterating the space for insertion of the dorsal process of cleithrum. Consequently, this cleithral process is also absent in *Paracanthopoma* and *Paravandellia*, and is reduced in *Arhinoglanis* and *Glanapteryx*.

Character 61 (state 1): medial process of supracleithrum absent (Figs. 3A, 6A). This apomorphic condition is homoplastically found in the tridentine clade of *Tridens*+*Tridensimilis*, *Arhinoglanis*, the vandelliine clade of *Paracanthopoma* + *Paravandellia*, at least *Sarcoglanis* within Sarcoglanidinae, and at least *Glanapteryx* within Glanapteryginae. This character is structurally correlated with the previously described character; however, a normal orifice receiving the dorsal process of cleithrum in the skull is still present in the clade *Tridens* + *Tridensimilis* and in *Sarcoglanis*. The body of the supracleithrum in *Tridens* is reduced to barely the ossification of the canal containing the postotic branch of the lateral line, lacking entirely the medial process; while in *Arhinoglanis* and *Paravandellia*, the process is lost as a result of the direct attachment of the supracleithrum to the basioccipital+exoccipitals, thus this character must be interpreted as independently acquired in these taxa.

Character 74 (state 1): ventral exposure of the epioccipital (Fig. 6A). The epioccipital typically forms the posterolateral corner of the dorsal bulge corresponding to the posterior semicircular canal, and articulates anteromedially with the supraoccipital, posteromedially with the exoccipital, and laterally with the pterotic, not extending ventrally because the shape of this last articulation leaves the posterior end of the pterotic free. In the derived state, the epioccipital extends laterally and its articulation with the pterotic reaches its posterior margin, so the epioccipital delimits the posterior margin of the pterotic and, therefore, the epioccipital is ventrally completely exposed in that region. This character is homoplastically present in *Bullockia*, *Eremophilus*, *Hatcheria*, *Trichomycterus caliensis*, *Cambeva ventropapillata*, *Ituglanis* sp., and *Scleronema macanuda* within Trichomycterinae, *Arhinoglanis*, and at least *Sarcoglanis* within Sarcoglanidinae.

Character 93 (state 0): posterolateral process of the pterotic absent (Figs. 3A, 6A). Homoplastic in *Glanapteryx* and best interpreted as independently reversed in *Arhinoglanis*, based on the distant phylogenetic position of both taxa.

Character 105 (state 0): relative length of the postzygapophysis of the complex vertebra. In the plesiomorphic character-state, the postzygapophysis of the complex vertebra reaches the anterior margin of the first post-Weberian vertebra (Fig. 9C) and this condition is homoplastically found in all trichomycterines examined (where this zygapophysis is present), and in *Acanthopoma*, *Arhinoglanis*, *Haemomaster*, *Megalocentor*, and *Stegophilus* within Stegophilinae, and at least *Sarcoglanis* within Sarcoglanidinae.

Character 214 (state 1): dorsal margin of quadrate convex or straight. This character was already described by DoNascimiento (2015), when it was formerly proposed as an autapomorphy for *Pseudostegophilus*, occurring homoplastically in *Arhinoglanis*.

Character 222 (state 1): posterodorsal process of hyomandibula absent (Fig. 9A). In the plesiomorphic condition, the hyomandibula has a posterior process on its dorsal margin (just posterior to the articular facet for the neurocranium), which is connected to the neurocranium through a ligament. This process is absent in the derived state, thus the posterodorsal corner of the hyomandibula coincides with the posterior end of the articular facet. This process is homoplastically absent in *Tridens* within Tridentinae, *Arhinoglanis* and the clade of *Apomatoceros* + *Megalocentor* within Stegophilinae, and at least *Sarcoglanis* within Sarcoglanidinae. In *Tridens*, the posterior end of the dorsal margin of the hyomandibula has a slightly convex contour; however, it keeps the ligament that connects to the pterotic, which is attached to the posterior margin of the hyomandibula.

Character 327 (state 1): medial tip of epibranchial 4 not expanded (Figs. 4, 8A). In the plesiomorphic character-state the medial tip of the epibranchial 4 is twice as wide or wider than the distal tip of the same epibranchial. The derived character-state is homoplastically distributed in several other stegophilines besides *Arhinoglanis* (*Apomatoceros*, *Haemomaster*, *Henonemus*, *Megalocentor*, *Ochmacanthus*, and *Stegophilus*), as well as in the vandelliines *Paravandellia* sp. (Orinoco) and an undescribed genus. In the examined specimen of *Pseudostegophilus* sp. (Madre de Dios), left epibranchial 4 is co-ossified with the corresponding pharyngobranchial and the associated tooth plate, retaining some cartilaginous centres to the ventral region. However, epibranchial 4 of *Tridens* is entirely cartilaginous, and has a triangular shape, with its medial tip wider than its lateral tip.

Character 330 (state 1): pharyngobranchial 3 not ossified (Fig. 4). A derived entirely cartilaginous pharyngobranchial 3 is found in *Tridentopsis*, *Arhinoglanis*, and *Pseudostegophilus haemomyzon*, while *Schultzichthys* was coded as polymorphic. Pharyngobranchial 3 in *Tridentopsis* and *Schultzichthys* keeps the morphology and topology observed for the same element in its ossified condition in remaining trichomycterids, i.e. a short cylindrical element, whose anterior tip is associated with the medial tip of epibranchial 2, and its posterior tip with the anterolateral tip of pharyngobranchial 4. In *Tridentopsis*, the anterior tip of pharyngobranchial 3 is characteristically oriented anterolaterally. In *Schultzichthys*, only two of four examined specimens (MBUCV-CT-916 and MBUCV-CT-920) have a single asymmetrically ossified pharyngobranchial, and in both cases on the left side. In the first specimen, the element is totally ossified, while in the second specimen, only a nodular portion at the medial tip of the circular cartilage is ossified and does not reach epibranchial 2. In the single specimen of *Pseudostegophilus maculatus*, pharyngobranchial 3 of the left side is missing, from which we can infer that some intraspecific variation exists. In the smaller examined specimen of *Pseudostegophilus* sp. (Orinoco and Essequibo), the third pharyngobranchial at both sides is completely cartilaginous, suggesting that this is one of the last elements to ossify in the branchial series.

Character 390 (state 1): increased number of upper procurrent caudal-fin rays (21–28 rays). *Arhinoglanis* has 21 rays, just at the lower limit of variation defined here for state 1, while *Homodiaetus* was coded as polymorphic for states 0 and 1, showing variation (16–21 rays) that encompasses the plesiomorphic character-state (6–20 rays). However, *Schultzichthys* has 9–16 rays, hence also corresponding to state 0. A more refined coding strategy is recommended for this and other meristic characters that were here treated as discrete states, where each character-state was defined based on gaps between ranges observed in the examined taxa.

Character 392 (state 1): increased number of lower procurrent caudal-fin rays (21–29 rays). A total of 23 procurrent rays were recorded in the single cs specimen of *Arhinoglanis*, where the exact number of these diminutive, slender, and poorly ossified structures could be confidently determined. As for the previous character, variation recorded in *Homodiaetus* (18–23) encompasses states 0 (8–19 rays) and 1 (21–29 rays), being consequently coded as polymorphic. The number of procurrent rays of *Schultzichthys* (8–13) corresponds to state 0.

Character 406 (state 1): increased number of procurrent dorsal-fin rays (more than two rays). *Nematogenys* has 1–2 dorsal-fin procurrent rays, thus a higher number is here considered apomorphic for Trichomycteridae. The derived condition has homoplastic distribution in *Bullockia*, *Hatcheria*, *Scleronema*, and *Henonemus taxistigmus* with three procurrent rays, *Ituglanis* sp. with four rays, *Eremophilus*, *Ochmacanthus flabelliferus*, *Ochmacanthus orinoco*, *Ochmacanthus reinhardtii*, *Paravandellia phaneronema*, and the undescribed genus of Vandelliinae with 5 rays, *Ochmacanthus* sp. with 6 rays, *Paravandellia* sp. (Caquetá) with 7 rays, while *Paracanthopoma irritans* and *Vandellia* have a range of variation of 4–5 rays, and *O. alternus* and *Paravandellia* sp. (Orinoco) have 4–6 rays. *Arhinoglanis* was coded as polymorphic, having 2 or 3 procurrent dorsal-fin rays.

Character 488 (state 2): exit of pterotic branch of postotic canal of cephalic laterosensory system from pterotic, adjacent to supracleithrum (Figs. 3A, 7A). Plesiomorphically, the pterotic branch emerges directly from the point of articulation between the pterotic and the supracleithrum, thus its exit foramen is surrounded by both bones. The pterotic branch in *Potamoglanis hasemani* emerges from the posterolateral shelf of the pterotic, giving the impression that its exit is exclusive to this bone; however, the foramen is dorsally delimited by both the pterotic and the supracleithrum, corresponding then to state 0 as defined here. In state 2, homoplastically recorded in *Arhinoglanis*, *Megalocentor*, and *Stegophilus* within Stegophilinae, the foramen is entirely framed by the pterotic. *Trichogenes*, *Bullockia*, and *Hatcheria* show another derived state (coded as 1), defined by the exit located at the anterior region of the supracleithrum. In *Pseudostegophilus maculatus*, the pterotic branch emerges exclusively from the pterotic, but its exit is anteriorly displaced, lying close and parallel to the preopercular canal (state 3), where the membranous canal that emerges immediately bends posteriorly at a right angle to continue parallel to the antero-posterior body axis. This character-state is also present in *Acanthopoma*, *Pareiodon*, and other evaluated species of *Pseudostegophilus*.

Character 503 (state 5): maximum number of labial tooth rows (six rows). *Miuroglanis platycephalus* (Tridentinae) and *Stegophilus septentrionalis* (Stegophilinae) have one row of labial teeth, suggesting that a single row of labial teeth constitutes the plesiomorphic condition, thus the increased number of rows was coded as a series of several successive derived states, according to the maximum number of tooth rows recorded in each species, although it does not imply a defined ordering in the analysis.

Sister group relationship of *Homodiaetus* and *Schultzichthys*

The clade formed by these two genera is supported by six characters, all showing homoplastic distribution:

Character 126 (state 1): notch on posterior margin of dentary (Fig. 6B). In the plesiomorphic character-state, the external surface of the posterior portion of the dentary is a wide lamina with a posteriorly convex or slightly emarginate edge, which covers most of the angular-articular-retroarticular bone, leaving exposed mostly just the articular portion of the latter. The apomorphic character-state is defined by a deep notch on the posterior margin, which can extend to the level of the internal articular facet of the dentary as seen in *Tridens* and *Tridensimilis*, giving rise to a pair of pointed posterior projections, with the dorsal projection slender and continuous with the base where mandibular teeth are inserted, and a long ventral process of variable width, which reaches the anterior margin of the coronoid portion of the angular-articular-retroarticular, resulting in a more laterally exposed surface of this latter bone. *Paravandellia phaneronema* has a lateral process on the angular-articular-retroarticular, which is anteriorly delimited by the posterior margin of the dentary, giving it an emarginate appearance. However, this condition is interpreted as independent from the emarginate margin observed in *Tridens* + *Tridensimilis*, *Ochmacanthus* (except *Ochmacanthus orinoco*), *Homodiaetus* + *Schultzichthys*, and most genera of the *Pareiodon* group (*Acanthopoma*, *Apomatoceros*, *Henonemus*, *Megalocentor*, and *Pseudostegophilus*), based on the absence of the aforementioned process of the angular-articular-retroarticular in these tridentines and stegophilines.

Character 158 (state 1): anterior margin of the premaxilla crenulate. The plesiomorphic condition is a smooth or an irregular edge of the premaxilla, while the derived state consists of a series of short but conspicuous finger-like extensions projecting in front of the insertion of the anteriormost row of teeth, being regularly spaced along the proximal portion of the anterior edge of the premaxilla, giving it a crenulate appearance. The derived state is homoplastic in *Homodiaetus* + *Schultzichthys*, and in most members of the *Pareiodon* group (*Acanthopoma*, *Apomatoceros*, *Henonemus*, *Megalocentor*, and *Pseudostegophilus*).

Character 228 (state 1): anterior end of preopercle inconspicuous. The preopercle in Siluriformes is a rather compact and stout bone, which mostly defines the ventral margin of the suspensory arch, articulating dorsally with the quadrate in its anterior region, and with the hyomandibula posteriorly, extending dorsally along the posterior margin of the hyomandibula as a tubular ossification, carrying the preoperculomandibular canal of the laterosensory system. In trichomycterids, the posterodorsal canal-bearing portion is missing, correlated with the incomplete preoperculomandibular canal. The anterior region of the preopercle corresponds to the portion placed anterior to the articulation with the interopercle, being generally pointed and firmly attached to the quadrate by an ankylosed articulation. In the derived state 1 (homoplastically recorded in the stegophilines *Homodiaetus* + *Schultzichthys*, *Apomatoceros*, *Henonemus*, *Pseudostegophilus maculatus*, and *Pseudostegophilus haemomyzon*), the anterior region of the preopercle is inconspicuous (not attenuated) from the articular region with the interopercle. In derived state 2 (autapomorphic for an undescribed genus of Vandelliinae), the anterior region is simply missing, resulting in the loss of articulation with the quadrate.

Character 263 (state 1): parurohyal with a midventral keel (Fig. 8B). This character has a homoplastic distribution restricted to stegophiline members: *Ochmacanthus*, *Homodiaetus* + *Schultzichthys*, and *Acanthopoma*, *Henonemus*, and *Pseudostegophilus* within the *Pareiodon* group).

Character 298 (state 1): basibranchial 4 and hypobranchial 3 fused. This character is homoplastically recorded in *Tridens*, *Haemomaster*, *Homodiaetus* + *Schultzichthys*, *Apomatoceros*, and *Henonemus punctatus*.

Miniaturization

Miniaturization is a phylogenetically widespread trend in animals (Hanken and Wake 1993) and Neotropical fishes reflect this, with more than 210 species among at least 25 teleostean families present in South American aquatic ecosystems (i.e. engraulids, crenuchids, lebiasinids, gasteropelecids, spintherobolids, stevardids, characids, acestrorhamphids, trichomycterids, callichthyids, scoloplacids, astroblepids, loricariids, cetopsids, aspredinids, auchenipterids, doradids, heptapterids, pseudopimelodids, eleotrids, gobiids, rivuliids, fluviphylacids, poeciliids, and cichlids) (Toledo-Piza *et al.* 2014). Except for *Trichomycterus santaeritae* (Eigenmann, 1918), all remaining miniature trichomycterids are members of the subfamilies Tridentinae, Stegophilinae, Vandelliinae, Sarcoglanidinae, Glanapteryginae, and Microcambevinae, the so-called TSVSGM-clade (Costa *et al.* 2020), where the subfamilies Tridentinae, Sarcoglanidinae, and Glanapteryginae (accepting that *Glanapteryx* and *Typhlobelus* are elongate miniatures) are exclusively represented by miniature species, while Vandelliinae and Microcambevinae (also admitting that *Listrura* species represent elongate miniatures) include several miniature species.

The only trichomycterid subfamily of the TSVSGM-clade that remained with no known miniatures was Stegophilinae, until the present discovery of *Arhinoglanis*. Toledo-Piza *et al.* (2014) had listed *Schultzichthys gracilis* as the sole miniature member of the Stegophilinae; however, this species attains 30 mm SL (as indicated for the skeletal length = SL of one of its paratypes in the original description of this species), thus exceeding the cut-off measure of 26 mm SL proposed by Weitzman and Vari (1988) to categorize Neotropical fish species as miniature. This inflexible size criterion is certainly unsatisfactory as the aforementioned authors do recognize and dismiss some obvious instances of phylogenetic miniaturization (e.g. *Belonion* among needlefishes and the glanapterygines and microcambevines above referred).

The largest specimen of *Arhinoglanis relictus* here recorded is 26.4 mm SL, which is within the miniature's threshold *sensu* Weitzman and Vari (1988). These authors also commented that many species attaining a maximum size of 26 mm SL, reach sex maturity

at under 20 mm SL. Given the few available specimens of *Arhinoglanis relictus*, we were only able to verify sexual maturity via direct examination of gonads in the single specimen selected for clearing and staining (21 mm SL). Developed gonads could not be observed in this specimen. However, the two specimens used to examine their osteology have a well-ossified neurocranium, comparable to that of remaining stegophilines, with an entirely closed skull roof (lacking fontanels), complete sutural joints between bones, and bones with well-defined osseus outer margins (Figs. 3A, 6A, 7A, 9), lacking cartilaginous or dermal connective tissue framing the borders (typical of early ontogenetic stages in trichomycterids) (de Pinna 1989). de Pinna (1989) also indicates that presence of ossified pectoral radials and hypobranchials are adult features in trichomycterids, and this is true for the single pectoral radial found in *Arhinoglanis* (Fig. 9C), but not for its three hypobranchials that remain cartilaginous (Fig. 4), with this last condition being another paedomorphic feature. Arratia (1990) finds that all bones constituting the suspensorium are well ossified at the end of ontogeny in *Trichomycterus areolatus*, and this condition is quite evident in *Arhinoglanis*, where compact and robust bones comprise the entire suspensorium and opercular series (Figs. 6A, 9).

Thus, these observations indicate that the examined specimens of *Arhinoglanis* are adults, despite their unverified gonadal development. Moreover, *Arhinoglanis relictus* also exhibits paedomorphic features, another attribute defining miniaturization. Paedomorphosis is particularly important in *Arhinoglanis*, considering that one of the most salient exclusive autapomorphies of the genus (dorsal lamina of mesethmoid unossified, Fig. 2A) is paedomorphic, as corroborated here in a strictly phylogenetic context. Following the developmental ossification sequence of the mesethmoid in *Schultzichthys* (one of two closest relatives of *Arhinoglanis*, the other being *Homodiaetus*), the dorsal lamina of the mesethmoid is the last structure to ossify, representing the final stage of ossification of this bone, as verified in a size-series of CT-scanned specimens of *Schultzichthys* (Fig. 13). Thus, the missing bony dorsal lamina of the mesethmoid in *Arhinoglanis* represents an event of developmental truncation, via terminal deletion of this last stage during ossification of the mesethmoid.

Another condition possibly representing a paedomorphic feature in *Arhinoglanis*, though showing homoplastic distribution in trichomyterids, is the unossified third pharyngobranchial (Fig. 4), which is present in the miniature *Tridentopsis*, but also in the non-miniatures *Pseudostegophilus haemomyzon* and *Schultzichthys*. However, this element has a relatively late ossification in the developmental sequence of branchial arches, as has been documented in phylogenetically distant clades of siluriforms, e.g. clariids (Adriaens and Verraes 1998) and ictalurids (Kubicek 2022). In fact, the third pharyngobranchial is the penultimate element to ossify in the branchial skeleton of *Clarias gariepinus* (Adriaens and Verraes 1998), followed by the fourth pharyngobranchial, which is phylogenetically lost in the clade of Stegophilinae + Vandelliinae. Except for the late ossification of basibranchials and hypobranchials in *Ictalurus punctatus* and *Noturus gyrinus* (Kubicek 2022), developmental sequences of branchial arch ossification are similar in Clariidae and Ictaluridae.

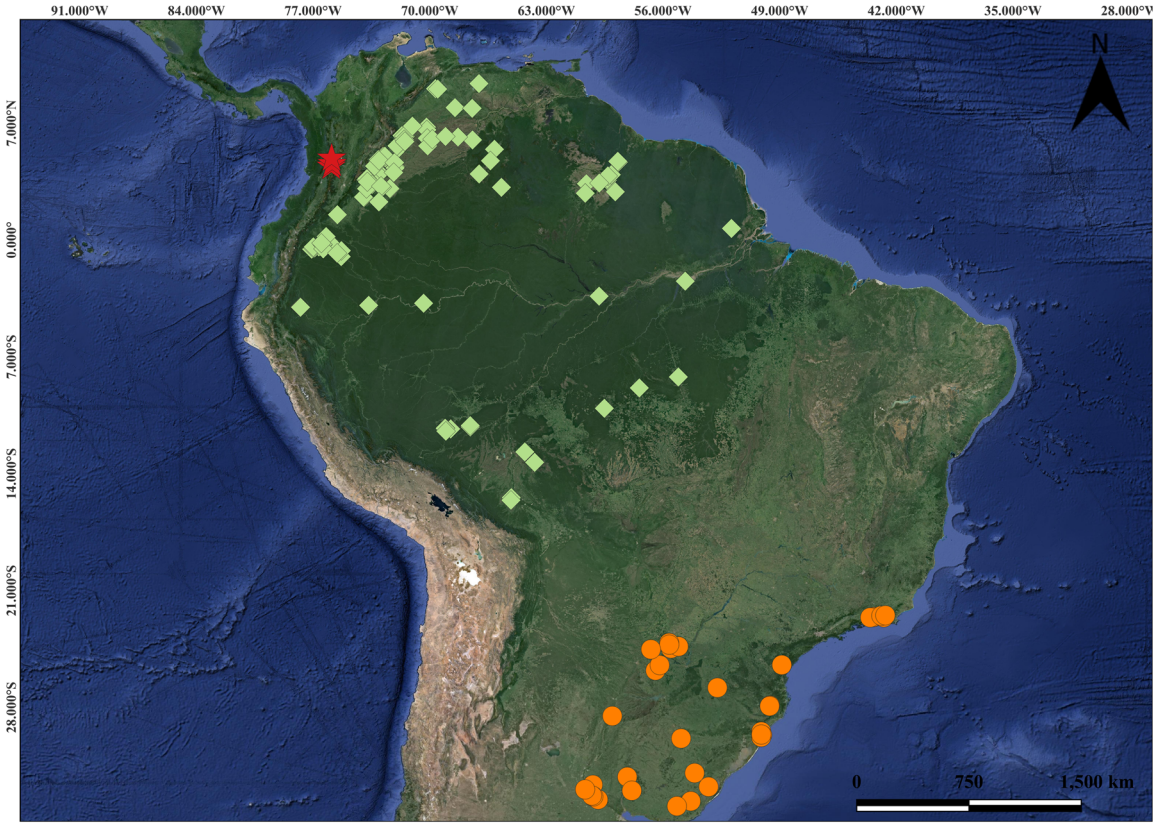

Figure 14. Geographic distribution of species of *Arhinoglanis* (stars), *Schultzichthys* (diamonds), and *Homodiaetus* (circles) in South America. Occurrence data from GBIF.org (15 September 2023).

Interestingly, *Arhinoglanis* additionally shows three character-states only shared with miniatures within Trichomycteridae, i.e. absence of a cranial orifice for insertion of the dorsal process of the cleithrum (Figs. 3A, 6A) (shared with *Paracanthopoma* + *Paravandellia*, and *Glanapteryx*), absence of the medial process of the supracleithrum (Figs. 3A, 6A) (shared with *Tridens* + *Tridensimilis*, *Paracanthopoma* + *Paravandellia*, *Sarcoglanis*, and *Glanapteryx*), and absence of the posterolateral process of the pterotic (Figs. 3A, 6A) (*Glanapteryx*). The latter two characters are clearly reductive, while the closure of the open space in the posterolateral corner of the neurocranium to receive the dorsal process of the cleithrum seems to be functionally associated with the loss of the medial process of the supracleithrum in *Arhinoglanis*, *Paracanthopoma* + *Paravandellia*, and *Glanapteryx*, each having independent evolutionary origin, based on the single most parsimonious topology obtained in our cladistic analysis of Trichomycteridae.

Biogeography

Arhinoglanis is further distinguished from other Stegophilinae by being the only genus to occur west of the Andes Mountains, exclusively having a so-called 'trans-Andean' distribution in the upper Cauca River drainage of Colombia (Fig. 14). Within the larger TSVSGM-clade, the only other subfamilies with trans-Andean representatives are Tridentinae and Vandelliinae, with a single species each (*Tridensimilis venezuelae* and *Paravandellia phaneronema*; DoNascimiento and de Pinna 2025). In contrast to the relatively wide distribution of these two species across their respective basins (Lake Maracaibo and Magdalena, respectively), *Arhinoglanis relictus* is restricted to the northernmost section of the upper Cauca River, where the river exits the valley to enter the canyon that defines the river channel along the entire middle Cauca River basin (Fig. 11).

The exceptionally restricted distribution of *Arhinoglanis relictus* is even more distinctive when compared to the combined distributions of members of its sister clade, *Homodiaetus* + *Schultzichthys*, which cover a vast area spanning all major cis-Andean basins (Fig. 14). *Schultzichthys* currently comprises only two species, *Schultzichthys gracilis* (type species) restricted to the Guaviare River drainage (Orinoco basin) (Bogotá-Gregory *et al.* 2022), and *Schultzichthys bondi* which is widely distributed in Greater Amazonia as defined by Van der Sleen and Albert (2018), having been originally described from the Orinoco basin, but also recorded from the Amazon (de Pinna and Wosiacki 2003, Wosiacki and de Pinna 2007) and Essequibo basins (Taphorn *et al.* 2022). *Homodiaetus* in turn has four species, *Homodiaetus anisitsi* (type species), which has the widest distribution within the genus, occurring in the lower Paraná, Uruguay, and Paraguay rivers, and smaller coastal basins of Rio Grande do Sul State in Brazil (Wosiacki and de Pinna 2007). The three other congeners have more restricted distributions in southeastern Brazil: *Homodiaetus graciosa* from the Morretes and Paranaguá rivers (Paraná State, Brazil) and the Ribeira do Iguape River (São Paulo State, Brazil). *Homodiaetus banguela* and *Homodiaetus passarellii* are restricted to a single river basin each in Rio de Janeiro State, Brazil, in the São João and Macacu rivers, respectively.

A general biogeographical pattern that is repeated with variation in multiple lineages of fishes distributed on both sides of the Andes, in the Magdalena and cis-Andean basins, emerges from our phylogenetic hypothesis, with a clear vicariant sequence in the *Arhinoglanis* + (*Schultzichthys* + *Homodiaetus*) clade: Magdalena + (Greater Amazonia + Paraná-Paraguay and southeastern Brazil). Other fish genera illustrating minor variations on this general pattern include genera of Myliobatiformes (*Potamotrygon*, Fontenelle *et al.* 2021), Characiformes (*Curimata* and *Cyphocharax*, Melo *et al.* 2021; *Cynopotamus*, Souza *et al.* 2022; *Brycon* and *Salminus*, Abe *et al.* 2014; *Megaleporinus*, Ramirez *et al.* 2017; *Prochilodus*, Frable *et al.* 2022), and Siluriformes (*Spatuloricaria*, Covain *et al.* 2016; *Ancistrus*, Lujan *et al.* 2015; *Lasiancistrus*, Poveda-Cuellar *et al.* 2023; *Panaque*, Lujan *et al.* 2017; *Ageneiosus*, Calegari *et al.* 2019; and *Pseudoplatystoma*, Torrico *et al.* 2009).

The minimum age of isolation of *Arhinoglanis* as a stegophiline relict in the Magdalena basin is hypothesized to be around 10–12 Mya, coinciding with the separation of the Magdalena basin from the proto-Orinoco by the initial rise of the Eastern Cordillera (Lundberg *et al.* 1998, Albert *et al.* 2006, Cassemiro *et al.* 2023), but considering its restricted distribution to the upper Cauca River basin, such isolation could be even older (Middle Eocene, 43 Mya), coincident with emergence of the Central Cordillera (Lundberg *et al.* 1998, Albert and Reis 2011, Rodríguez-Olarte *et al.* 2011, Pérez-Consuegra *et al.* 2022). Notably, and despite the large departure of their Stegophilinae intrarelationships from most previous studies, the age estimate obtained by Tagliacollo *et al.* (2024) for the branch leading to *Homodiaetus* is 43.2 Mya. More research into temporal diversification dynamics of the TSVSGM-clade is needed to provide a more precise and robust assessment of the biogeographical origin of *Arhinoglanis*.

ACKNOWLEDGMENTS

José Luis Londoño López (GIUA) took and edited photographs of the holotype. Miguel Ángel Hernández-Cortés (Unidad Ejecutora Lillo - Fundación Miguel Lillo) edited Figures 1 and 11.

SUPPLEMENTARY DATA

Supplementary data is available at *Zoological Journal of the Linnean Society* online.

CONFLICT OF INTEREST

The authors declare no conflicts of interest related to the present work.

FUNDING

C.R.-V. thanks Corporación Autónoma Regional del Quindío (Julián Serna Giraldo) and Universidad del Quindío—Facultad de Investigaciones (Project 136) for funding fieldwork in 1996 that yielded specimens of *Arhinoglanis relictus*; IDEA WILD for donation of field equipment; and COLCIENCIAS for financial support through a predoctoral grant. Financial support to N.K.L. was provided by the Coypu Foundation and a Discovery Grant awarded by the Natural Sciences and Engineering Research Council of Canada. A.O-.L. thanks Corporación Autónoma Regional del Valle del Cauca—CVC (Pedro Nel Montoya) and Fundación FUNINDES Colombia (Convenio de Asociación No. 0022 of 2021) for funding fieldwork.

DATA AVAILABILITY

The data underlying this article are available in the article and in its online supplementary material.

REFERENCES

Abe KT, Mariguela TC, Avelino GS *et al.* Systematic and historical biogeography of the Bryconidae (Ostariophysi: Characiformes) suggesting a new rearrangement of its genera and an old origin of Mesoamerican ichthyofauna. *BMC Evolutionary Biology* 2014;**14**:152. https://doi.org/10.1186/1471-2148-14-152

Adriaens D, Verraes W. Ontogeny of the osteocranium in the African catfish, *Clarias gariepinus* Burchell (1822) (Siluriformes: Clariidae): ossification sequence as a response to functional demands. *Journal of Morphology* 1998;**235**:183–237.

Adriaens D, Baskin JN, Coppens H. Evolutionary morphology of trichomycterid catfishes: about hanging on and digging in. In: Nelson JS, Schultze HP, Wilson MVH (eds), *Origin and Phylogenetic Interrelationships of Teleosts*. München, Germany: Verlag Dr Friedrich Pfeil, 2010, 337–62.

Albert JS, Reis RE. Introduction to Neotropical freshwaters. In: Albert JS, Reis RE (eds), *Historical Biogeography of Neotropical Freshwater Fishes*. Berkeley and Los Angeles, California, USA: University of California Press, 2011, 3–19.

Albert JS, Lovejoy NR, Crampton WGR. Miocene tectonism and the separation of cis- and trans-Andean river basins: evidence from Neotropical fishes. *Journal of South American Earth Sciences* 2006;**21**:14–27. https://doi.org/10.1016/j.jsames.2005.07.010

Arcila D, Ortí G, Vari RP *et al.* Genome-wide interrogation advances resolution of recalcitrant groups in the tree of life. *Nature Ecology & Evolution* 2017;**1**:20. https://doi.org/10.1038/s41559-016-0020

Arratia G. Development and diversity of the suspensorium of trichomycterids and comparison with loricarioids (Teleostei: Siluriformes). *Journal of Morphology* 1990;**205**:193–218.

Bachman S, Moat J, Hill AW *et al.* Supporting Red List threat assessments with GeoCAT: geospatial conservation assessment tool. *ZooKeys* 2011;**150**:117–26. https://doi.org/10.3897/zookeys.150.2109

Bachman S, Moat J. GeoCAT—an open-source tool for rapid Red List assessments. *BGjournal* 2012;**9**:11–3. https://www.jstor.org/stable/24811237

Baskin JN. Structure and relationships of the Trichomycteridae. Unpublished Ph.D. Thesis. City University of New York, 1973.

Bauer IL. Candiru—a little fish with bad habits: need travel health professionals worry? A review. *Journal of Travel Medicine* 2013;**20**:119–24.

Betancur-R R, Wiley EO, Arratia G *et al.* Phylogenetic classification of bony fishes. *BMC Evolutionary Biology* 2017;**17**:162. https://doi.org/10.1186/s12862-017-0958-3

Bogotá-Gregory JD, DoNascimiento C, Lima FCT *et al.* Fishes from the Colombian Amazonia region: species composition from the river systems within the rainforest biome. *Biota Neotropica* 2022;**22**:e20221392. https://doi.org/10.1590/1676-0611-BN-2022-1392

Bonato KO, Silva PC, Malabarba LR. Unrevealing parasitic trophic interactions—a molecular approach for fluid-feeding fishes. *Frontiers in Ecology and Evolution* 2018;**6**:22. https://doi.org/10.3389/fevo.2018.00022

Calegari BB, Vari RP, Reis RE. Phylogenetic systematics of the driftwood catfishes (Siluriformes: Auchenipteridae): a combined morphological and molecular analysis. *Zoological Journal of the Linnean Society* 2019;**187**:661–773. https://doi.org/10.1093/zoolinnean/zlz036

Cassemiro FAS, Albert JS, Antonelli A *et al.* Landscape dynamics and diversification of the megadiverse South American freshwater fish fauna. *Proceedings of the National Academy of Sciences of the United States of America* 2023;**120**:e2211974120. https://doi.org/10.1073/pnas.2211974120

Costa WJEM, Henschel E, Katz AM. Multigene phylogeny reveals convergent evolution in small interstitial catfishes from the Amazon and Atlantic forests (Siluriformes: Trichomycteridae). *Zoologica Scripta* 2020;**49**:159–73. https://doi.org/10.1111/zsc.12403

Covain R, Fisch-Muller S, Oliveira C *et al.* Molecular phylogeny of the highly diversified catfish subfamily Loricariinae (Siluriformes, Loricariidae) reveals incongruences with morphological classification. *Molecular Phylogenetics and Evolution* 2016;**94**:492–517. https://doi.org/10.1016/j.ympev.2015.10.018

Datovo A, Bockmann FA. Dorsolateral head muscles of the catfish families Nematogenyidae and Trichomycteridae (Siluriformes: Loricarioidei): comparative anatomy and phylogenetic analysis. *Neotropical Ichthyology* 2010;**8**:193–246.

Datovo A, de Aquino PPU, Langeani F. A new species of *Ituglanis* (Siluriformes: Trichomycteridae) from the Tocantins and Paranaíba river basins, central Brazil, with remarks on the systematics of the genus. *Zootaxa* 2016;**4171**:439–58.

DoNascimiento C. Sistemática y relaciones filogenéticas de la subfamilia de bagres parásitos Stegophilinae (Siluriformes, Trichomycteridae). Unpublished PhD dissertation. Universidad Central de Venezuela, 2013.

DoNascimiento C. Monophyly of the subfamily of parasitic catfishes Stegophilinae (Siluriformes, Trichomycteridae) and phylogenetic diagnoses of its genera. *Copeia* 2015;**103**:933–60. https://doi.org/10.1643/CI-14-132

DoNascimiento C, de Pinna MCC. Parasitic catfishes. In: Arratia G, Reis RE (eds), *Catfishes, a Highly Diversified Group, Volume 1: Catfishes, and Their Outstanding Biology*. Boca Raton, Florida, USA: Science Publishers, 2025, 232–48.

DoNascimiento C, Prada-Pedreros S, Guerrero-Kommritz J. *Trichomycterus venulosus* (Steindachner, 1915), a junior synonym of *Eremophilus mutisii* Humboldt, 1805 (Siluriformes: Trichomycteridae) and not an extinct species. *Neotropical Ichthyology* 2014a;**12**:707–15.

DoNascimiento C, Prada-Pedreros S, Guerrero-Kommritz J. A new catfish species of the genus *Trichomycterus* (Siluriformes: Trichomycteridae) from the Río Orinoco versant of Páramo de Cruz Verde, Eastern Cordillera of Colombia. *Neotropical Ichthyology* 2014b;**12**:717–28.

DoNascimiento C, Provenzano F. The genus *Henonemus* (Siluriformes: Trichomycteridae) with a description of a new species from Venezuela. *Copeia* 2006;**2006**:198–205.

Fernández L, Schaefer SA. Relationships among the Neotropical candirus (Trichomycteridae, Siluriformes) and the evolution of parasitism based on analysis of mitochondrial and nuclear gene sequences. *Molecular Phylogenetics and Evolution* 2009;**52**:416–23.

Fontenelle JP, Marques FPL, Kolmann MA *et al.* Biogeography of the Neotropical freshwater stingrays (Myliobatiformes: Potamotrygoninae) reveals effects of continent-scale paleogeographic change and drainage evolution. *Journal of Biogeography* 2021;**48**:1406–19. https://doi.org/10.1111/jbi.14086

Frable BW, Melo BF, Fontenelle JP *et al.* Biogeographic reconstruction of the migratory Neotropical fish family Prochilodontidae (Teleostei: Characiformes). *Zoologica Scripta* 2022;**51**:348–64. https://doi.org/10.1111/zsc.12531

Goloboff PA, Morales ME. TNT version 1.6, with a graphical interface for MacOS and Linux, including new routines in parallel. *Cladistics: The International Journal of the Willi Hennig Society* 2023;**39**:144–53. https://doi.org/10.1111/cla.12524

Hanken J, Wake DB. Miniaturization of body size: Organismal consequences and evolutionary significance. *Annual Review of Ecology and Systematics* 1993;**24**:501–19.

International Union for Conservation of Nature (IUCN). Standards and Petitions Committee of the IUCN Species Survival Commission. Guidelines for using the IUCN Red List categories and criteria (Version 16), 2024. http://www.iucnredlist.org/documents/RedListGuidelines.pdf (12 April 2025, date last accessed).

Koch WR. Revisão taxonômica do gênero *Homodiaetus* (Teleostei, Siluriformes, Trichomycteridae). *Iheringia. Série Zoologia* 2002;**92**:33–46.

Kubicek KM. Developmental osteology of *Ictalurus punctatus* and *Noturus gyrinus* (Siluriformes: Ictaluridae) with a discussion of siluriform bone

homologies. *Vertebrate Zoology* 2022;**72**:661–727. https://doi.org/10.3897/vz.72.e85144

Lujan NK, Armbruster JW, Lovejoy NR *et al.* Multilocus molecular phylogeny of the suckermouth armored catfishes (Siluriformes: Loricariidae) with a focus on subfamily Hypostominae. *Molecular Phylogenetics and Evolution* 2015;**82(A)**:269–88. https://doi.org/10.1016/j.ympev.2014.08.020

Lujan NK, Cramer CA, Covain R *et al.* Multilocus molecular phylogeny of the ornamental wood-eating catfishes (Siluriformes, Loricariidae, *Panaqolus* and *Panaque*) reveals undescribed diversity and parapatric clades. *Molecular Phylogenetics and Evolution* 2017;**109**:321–36. https://doi.org/10.1016/j.ympev.2016.12.040

Lundberg JG, Marshall LG, Guerrero J *et al.* The stage for Neotropical fish diversifications: a history of tropical South American rivers. In: Malabarba LR, Reis RE, Vari RP *et al.* (eds), *Phylogeny and Classification of Neotropical Fishes*. Porto Alegre, Brazil: EDIPUCRS, 1998, 13–48.

Lundberg JG, Baskin JN. The caudal skeleton of the catfishes, order Siluriformes. *American Museum Novitates* 1969;**2398**:1–49.

Maddison WP, Maddison DR. Mesquite: a modular system for evolutionary analysis (Version 4.02). 2025. http://www.mesquiteproject.org (12 April 2025, date last accessed).

Melo BF, Albert JS, Dagosta FCP *et al.* Biogeography of curimatid fishes reveals multiple lowland–upland river transitions and differential diversification in the Neotropics (Teleostei, Curimatidae). *Ecology and Evolution* 2021;**11**:15815–32. https://doi.org/10.1002/ece3.8251

de Miranda Ribeiro P. Notas para o estudo dos Pygidiidae brasileiros (Pisces—Pygidiidae—Stegophilinae), I. *Boletim do Museu Nacional do Rio de Janeiro, Nova Série, Zoologia* 1946;**58**:1–20.

Ochoa LE, Datovo A, DoNascimiento C *et al.* Phylogenomic analysis of trichomycterid catfishes (Teleostei: Siluriformes) inferred from ultraconserved elements. *Scientific Reports* 2020;**10**:2697. https://doi.org/10.1038/s41598-020-59519-w

Ortega-Lara A, Ospina V, Reyes MP *et al.* Guía de campo para la identificación de los peces de la cuenca alta del río Cauca. Corporación Autónoma Regional del Valle del Cauca (CVC) and Fundación para la Investigación y el Desarrollo Sostenible (FUNINDES). Santiago de Cali, Colombia: Alfagraphic E.U., 2022a.

Ortega-Lara A, Rockstroh P, Salcedo-Portilla C *et al.* Peces del alto Cauca: orígenes, diversidad y conservación. Corporación Autónoma Regional del Valle del Cauca (CVC) and Fundación para la Investigación y el Desarrollo Sostenible (FUNINDES). Santiago de Cali, Colombia: Alfagraphic E.U., 2022b.

Pérez-Consuegra N, Hoke GD, Fitzgerald P *et al.* Late Miocene–Pliocene onset of fluvial incision of the Cauca River Canyon in the Northern Andes. *GSA Bulletin* 2022;**134**:2453–68. https://doi.org/10.1130/B36047.1

de Pinna MCC. A new scarcoglanidine catfish, phylogeny of its subfamily, and an appraisal of the phyletic status of the Trichomycterinae (Teleostei, Trichomycteridae). *American Museum Novitates* 1989;**2950**:1–39.

de Pinna MCC. A new subfamily of Trichomycteridae (Teleostei, Siluriformes), lower loricarioid relationships and a discussion on the impact of additional taxa for phylogenetic analysis. *Zoological Journal of the Linnean Society* 1992;**106**:175–229.

de Pinna MCC. Phylogenetic relationships of Neotropical Siluriformes: historical overview and synthesis of hypotheses. In: LR Malabarba, RE Reis, RP Vari *et al.* (eds), *Phylogeny and Classification of Neotropical Fishes*. Porto Alegre, Brazil: EDIPUCRS, 1998; 279–330.

de Pinna M. Trichomycteridae. In: de Queiroz LJ, Torrente-Vilara G, Massaharu WO *et al.* (eds), *Peces do Rio Madeira*, Vol. II. São Paulo, Brazil: Santo Antônio Energía, 2013, 142–79.

de Pinna MCC, Britski HA. *Megalocentor*, a new genus of parasitic catfish from the Amazon basin: the sister group of *Apomatoceros* (Trichomycteridae: Stegophilinae). *Ichthyological Exploration of Freshwaters* 1991;**2**:113–28.

de Pinna M, Dagosta FCP. A taxonomic review of the vampire catfish genus *Paracanthopoma* Giltay, 1935 (Siluriformes, Trichomycteridae), with descriptions of nine new species and a revised diagnosis of the genus. *Papéis Avulsos de Zoologia* 2022;**62**:e202262072.

de Pinna MCC, Wosiacki W. Family Trichomycteridae (Pencil or parasitic catfishes). In: Reis RE, Kullander SO, Ferraris CJ Jr. (eds), *Checklist of the Freshwater Fishes of South and Central America*. Porto Alegre, Brazil: EDIPUCRS, 2003, 270–90.

de Pinna M, Reis V, Britski HA. A new species of *Trichogenes* (Siluriformes, Trichomycteridae), with a discussion on the homologies of the anterior orbital bones in trichomycterids and other loricarioids. *American Museum Novitates* 2020;**2020**:1–27.

Poveda-Cuellar JL, Conde-Saldaña CC, Villa-Navarro FA *et al.* Phylogenetic revision of whisker-cheeked suckermouth catfishes (Loricariidae: *Lasiancistrus*) from east of the Andes: five species where once there were two. *Zoological Journal of the Linnean Society* 2023;**199**:688–712. https://doi.org/10.1093/zoolinnean/zlad042

Ramirez JL, Birindelli JL, Carvalho DC *et al.* Revealing hidden diversity of the underestimated Neotropical ichthyofauna: DNA barcoding in the recently described genus *Megaleporinus* (Characiformes: Anostomidae). *Frontiers in Genetics* 2017;**8**:149. https://doi.org/10.3389/fgene.2017.00149

Rodríguez-Olarte D, Mojica Corzo JI, Taphorn Baechle DC. Northern South America: Magdalena and Maracaibo basins. In: Albert JS, Reis RE (eds), *Historical Biogeography of Neotropical Freshwater Fishes*. Berkeley and Los Angeles, California, USA: University of California Press, 2011, 243–257.

Román-Valencia C, Ruiz-C RI, Taphorn DC *et al. Guía para la identificación de los peces del río La Vieja*. Alto Cauca, Colombia: Eumed, 2018.

Sabaj MH. Codes for natural history collections in ichthyology and herpetology (online supplement) (Version 9.0, 14 February 2022). American Society of Ichthyologists and Herpetologists. 2022. https://asih.org (12 April 2025, date last accessed).

Sidlauskas BL, Vari RP. Phylogenetic relationships within the South American fish family Anostomidae (Teleostei, Ostariophysi, Characiformes). *Zoological Journal of the Linnean Society* 2008;**154**:70–210.

Souza CS, Melo BF, Mattox GMT *et al.* Phylogenomic analysis of the Neotropical fish subfamily Characinae using ultraconserved elements (Teleostei: Characidae). *Molecular Phylogenetics and Evolution* 2022;**171**:107462. https://doi.org/10.1016/j.ympev.2022.107462

Spotte S, Petry P, Zuanon JAS. Experiments on the feeding behavior of the hematophagous candiru, *Vandellia* cf *plazaii*. *Environmental Biology of Fishes* 2001;**60**:459–64.

Tagliacollo VA, Tan M, Reis RE *et al.* Time-calibrated phylogeny of Neotropical freshwater fishes. *Frontiers in Bioinformatics* 2024;**4**:1433995. https://doi.org/10.3389/fbinf.2024.1433995

Taphorn DC, Liverpool E, Lujan NK *et al.* Annotated checklist of the primarily freshwater fishes of Guyana. *Proceedings of the Academy of Natural Sciences of Philadelphia* 2022;**168**:1–95. https://doi.org/10.1635/053.168.0101

Toledo-Piza M, Mattox GMT, Britz R. *Priocharax nanus*, a new miniature characid from the Rio Negro, Amazon basin (Ostariophysi: Characiformes). *Neotropical Ichthyology* 2014;**12**:229–46. https://doi.org/10.1590/1982-0224-20130171

Torrico JP, Hubert N, Desmarais E *et al.* Molecular phylogeny of the genus *Pseudoplatystoma* (Bleeker, 1862): biogeographic and evolutionary implications. *Molecular Phylogenetics and Evolution* 2009;**51**:588–94. https://doi.org/10.1016/j.ympev.2008.11.019

Van der Sleen P, Albert JS. *Field Guide to the Fishes of the Amazon, Orinoco, and Guianas*. Princeton, New Jersey, USA: Princeton University Press, 2018.

Weitzman SH, Vari RP. Miniaturization in South American freshwater fishes: an overview and discussion. *Proceedings of the Biological Society of Washington* 1988;**101**:444–65.

Wosiacki WB, de Pinna MCC. Família Trichomycteridae: Stegophilinae. In: Buckup PA, Menezes NA, Ghazzi MS (eds), *Catálogo das espécies de peixes de água doce do Brasil*, Vol. **23**. Série Livros. Museu Nacional, Universidade Federal do Rio de Janeiro, 2007, 72–3.